CORROSION MONITORING OF METAL ALLOYS USING A LINE-FOCUS ULTRASONIC TRANSDUCER SYSTEM

by

Menghan Jiang

Bachelor of Engineering, Tianjin University, 2017

Submitted to the Graduate Faculty of

Swanson School of Engineering in partial fulfillment

of the requirements for the degree of

Master of Science in Mechanical Engineering

University of Pittsburgh

2019

UNIVERSITY OF PITTSBURGH

SWANSON SCHOOL OF ENGINEERING

This thesis was presented

by

Menghan Jiang

It was defended on

April 4, 2019

and approved by

Qing-Ming Wang, Ph.D., Professor

Department of Mechanical Engineering and Materials Science

Heng Ban, Ph.D., Professor

Department of Mechanical Engineering and Materials Science

Xiayun Zhao, Ph.D., Assistant Professor

Department of Mechanical Engineering and Materials Science

Thesis Advisor: Qing-Ming Wang, Ph.D., Professor

Department of Mechanical Engineering and Materials Science

CORROSION MONITORING OF METAL ALLOYS USING A LINE-FOCUS ULTRASONIC TRANSDUCER SYSTEM

Menghan Jiang, M.S.

University of Pittsburgh, 2019

Ultrasonic testing is a conventional non-destructive testing method and is considered as a promising approach for corrosion monitoring. The fundamental principles of ultrasonic testing in structural health monitoring have been studied comprehensively in the past decades. In this research, a line-focus PVDF ultrasonic transducer was designed, fabricated and applied to measure the Rayleigh surface wave velocity changes of some commercially available metal alloys during 5, 10, 15, 20 and 25 days of laboratory corrosion studies. The metal alloys investigated include 304 stainless steel, low-carbon steel, 6061 aluminum alloy, and multipurpose 110 copper. The corrosion tests were conducted by simulating these metal alloys subjected to seawater corrosion processing. For isotropic solid materials, the effective elastic modulus (Young's modulus) can be indirectly characterized from the experimental measurement of the Rayleigh surface wave velocity. The experimental data acquired by the line-focus ultrasonic transducer system were analyzed, from which it was found that the values of Rayleigh surface wave velocities and the Young's modulus decrease for 304 stainless steel, low-carbon steel and multipurpose 110 copper samples, while increase for 6061 aluminum alloy as the corrosion time increases during the experimental period. Clearly, the changing pattern of Rayleigh surface wave velocity of each of the metal alloys during corrosion processing could provide part of the predictive solutions for assessment and mitigation of corrosion; and the line-focus transducer system is promising for real-time monitoring of corrosion processes.

TABLE OF CONTENTS

LIST OF TABLES

LIST OF FIGURES

ACKNOWLEDGEMENT

Time flies by, my nearly two-years graduate study for master's degree is about to come to an end. During these days, I spent a great time in the University of Pittsburgh and learned a lot. Now I would like to express my sincere gratitude and best wishes to all those who care and support me.

First of all, I would like to sincerely thank my advisor, Dr. Qing-Ming Wang who always gave me meticulous guidance in a responsible manner, helped me to develop ideas and solve problems encountered in the research. In the meanwhile, I would like to express my thanks to my committee members: Dr. Heng Ban and Dr. Xiayun Zhao, for their time and patience to make this thesis better.

Secondly, my thanks to my research group members: Qiuyan Li and Chenglong Ji who has graduated. Also, thank all my research group member. This thesis would not be completed without their experience sharing and guidance.

In addition, I would like to thank my parents. Their encouragement and support all the time gave me the power to accomplish the end task.

I also sincerely thank everyone who helped me directly or indirectly during these days.

1.0 INTRODUCTION

With the large-scale application of metals and metal alloys in marine engineering, especially on ship structure, studying the corrosion behavior of metals and metal alloys is of great significance for marine structural design and material selection. In addition to the marine field, metals are also widely used in other areas that have corrosive environments. For example, in the medical field, implants, such as elbow and knee joints, are expected to be resistant to corrosion and have similar mechanical properties with bone. Immersion corrosion test is one of the most commonly used method to study the corrosion performance of various metal alloys. The immersion tests are mostly done in electrolytes such as acids and neutral saline solutions [1,2].

For metal corrosion, the current detection and monitoring technologies are mainly divided into direct intrusive corrosion monitoring techniques, direct non-intrusive techniques and indirect non-intrusive techniques. Among them, the non-intrusive techniques have the advantages of not damaging the article, saving time and money and high reliability. Ultrasonic corrosion monitoring is one of the commonly used non-intrusive techniques for corrosion monitoring. In this technique, high frequency acoustic waves are used to measure or map the surface and internal structure, thickness and other physical properties of testing articles [3].

This article reports on preliminary results concerning changes in mechanical properties with proceeding corrosion of several common metals including low-carbon steel, 304 stainless steel, 6061 aluminum and multipurpose 110 copper during their long-term exposure to acidic saline solution monitored by line-focused ultrasonic transducer.

1.1 NON-DESTRUCTIVE TESTING METHODS

There are a wide range of measurement techniques that have been used for corrosion monitoring. Among these techniques, non-destructive testing (NDT) methods are the most effective and widely used testing methods. Non-destructive testing is a means of testing the surface and internal quality of the part without damaging the working condition of the workpiece or raw material. Non-destructive testing methods for corrosion monitoring include radiographic testing, electromagnetic testing, guided wave testing and ultrasonic testing [4]. Ultrasonic testing is the testing method that I am focused on and will be fully discussed in this paper.

1.2 CURRENT ULTRASONIC CORROSION MONITORING TECHNIQUES

Ultrasound is a sound wave with a frequency higher than 20 kHz. Ultrasonic Testing, abbreviated as UT, is an ultrasonic scanning technique and is one of the conventional non-destructive testing methods. Ultrasonic testing is widely used in engineering applications such as flaw detection, dimensional measurements, material characterization and so on. Besides, it is also used in medical field such as medical imaging and stone breaking.

For corrosion monitoring, the biggest application of ultrasonic testing is ultrasonic echo-impulse method. This method is mainly used for determining the thickness thinning and characterization of discontinuity encountered in general and pitting corrosion. The ultrasonic echo-impulse method is based on the ultrasonic pulse reflection principle. When the ultrasonic pulse emitted by the probe passes through the measured object and reach the material interface,

the pulse is reflected back to the probe. By measuring the time of the ultrasonic wave propagating in the material, the thickness of the material can then be calculated.

Conventional technique for general corrosion testing only gives the wall thinning of the testing object but does not give information on the geometric dimensions of damage such as depth and correlation length of corroded profile [5]. Another testing method called ultrasonic flaw detection technology can solve this problem. Ultrasonic flaw detection technology is a technique that uses ultrasonic energy to penetrate into the interior of a metal material and enters the other side through one side and reflects at the edge of the interface to check whether the part has defects. The transmitter and receiver can analyze the reflected wave to accurately measure the defect and display the position and size of the internal defect.

1.3 LINE FOCUSED ULTRASONIC TRANSDUCER

1.3.1 Piezoelectric material

A commonly used ultrasonic transducer consists of a piezoelectric element that can emit as well as receive ultrasonic waves. This kind of ultrasonic transducer works by using the piezoelectric effect of piezoelectric materials. Piezoelectric effect is divided into the direct piezoelectric effect and the converse piezoelectric effect. When mechanical stress is applied to piezoelectric material, a shifting of the positive and negative charge centers in the material takes place and then results in an external electrical field. This effect is called the direct piezoelectric effect, which is the principle of ultrasonic transmission. When reversed, an outer electrical field

generates stress on the piezoelectric material. This effect is called the converse piezoelectric effect, which is used in ultrasonic reception.

1.3.2 Line-focus ultrasonic wave transducer

A surface acoustic wave (SAW) is a wave which travels along the material surface that exhibits elasticity and amplitude of material. In the 1990s, surface wave acoustic microscopy has been successfully developed and a large number of investigators have improved our knowledge of surface acoustic microscopy so today it is one of the most versatile methods to study the materials characterization. The output of piezoelectric transducer called $V(z)$curve is a record of the echo-interference amplitude V versus the distance z between probe and sample [6]. The periodicity of the $V(z)$ curve is directly related to the Rayleigh wave velocity. By analyzing these $V(z)$ curves, the material properties can be measured. Since that an acoustic microscope can be a quantitative tool for measurement of local elastic property [7].

In 1985 the first line-focus-beam (LFB) transducer for the acoustic microscope system was developed by Kushibiki. They developed a method of material characterization by means of the line-focus-beam acoustic microscope system with high measurement accuracy. By measuring the propagation characteristics of leaky waves on the water-sample boundary, the material properties are determined through V(z) curve measurements. Since then, more improved lenses and transducers have been developed such as the V-groove lens and the butterfly transducer.

Generally, the acoustic microscopes utilize small aperture lenses and high frequency tone bursts and have high spatial resolution capability which can cause high costs. In addition, the ratio of focal length to aperture called f number has to be low to generate leaky surface waves efficiently. Thus, a lens-less line-focus PVDF transducer with a large aperture and low f number

was developed by D. Xiang. Much of the design of the transducer in this paper refers to the work of Dan Xiang [8]. A line focused ultrasonic wave transducer has been used to determine material properties, such as Rayleigh surface wave velocity, elastic constant, and so on.

1.4 MOTIVATION

Metals and alloys are used in a wide variety of applications because of their high strength and ductility. However, metals in most environments are thermodynamically unstable and corrosive. Thus, corrosion monitoring methods are of vital importance and necessary to ensure the industry safety. Ultrasonic corrosion testing has the advantages of wide application range, strong penetrating power, high sensitivity, accurate determination of the depth position of the defect, easy carrying of the device, and harmlessness to the human body. Traditional ultrasonic corrosion monitoring method using echo-impulse technique can determine the thickness and detect the flaw of the metal parts. To improve the ultrasonic corrosion monitoring methods, a line-focus ultrasonic wave transducer based on the Rayleigh surface wave is introduced. By analyzing the Rayleigh wave, not only the thickness information but also the elastic properties of the object being tested can be obtained. This technique can increase the dimension of the corrosion degree evaluation and is possible to be applied in a wider range of practical field.

2.0 THEORETICAL BACKGROUND

The calculation method for elastic properties of metals is undoubtedly significant for evaluating the degree of corrosion and design of ultrasonic transducers. In this chapter, the basic formula derivation of commonly used elastic parameters and relationship between velocities of acoustic waves and Young's modulus will be illustrated. Besides, the theoretical principle of line-focused transducer measurement and chemical corrosion mechanism will be fully explained.

2.1 PHYSICAL PRINCIPLES OF ULTRASONIC TESTING

2.1.1 Mechanical waves

Ultrasonic testing is based on mechanical waves. Mechanical waves are generated by the vibration in materials. All materials are composed of discrete particles. During the propagation of mechanical waves, each discrete particle oscillates about their equilibrium positions, it only performs a simple harmonic motion of up and down (left and right), that is, the particle itself does not move forward with the propagation of mechanical waves.

Figure 1 shows the instantaneous picture of a wave travelling from left to right which has not reached the right edge in a model. The picture shows that the particles oscillate left and right around their equilibrium positions and create zones where the particles are closed to each other and zones where the particles are relatively far from each other. These compression zones and

rarified zones are constantly recreated on the left side and travel in the body at constant velocity and uniform intervals towards the right side. This process generates the elastic waves [9].

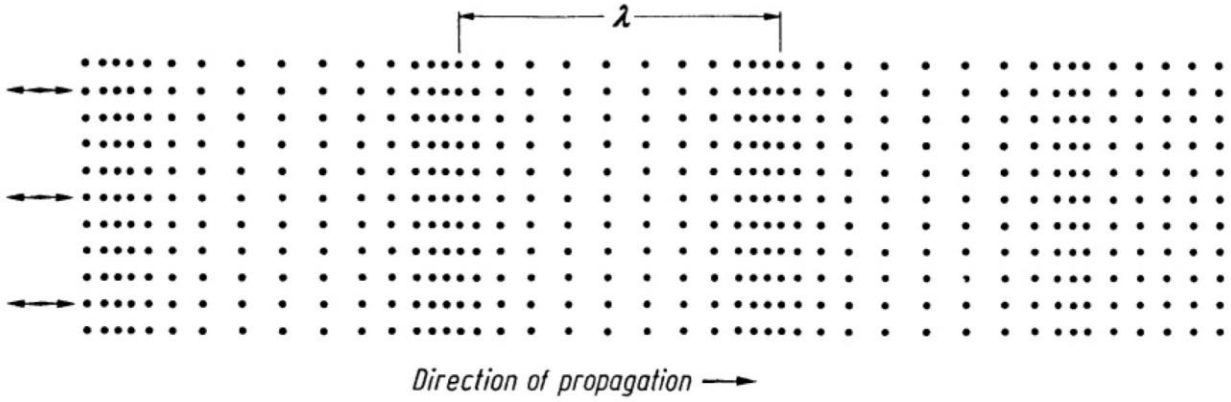

Figure 1. Longitudinal wave [9]

The wave described in Figure 1 is called a longitudinal wave because the vibration direction is consistent or parallel with the direction of propagation, which is also the longitudinal direction. Since compression and expansion forces are active in it, it is also called pressure or compression wave. Sound wave is a common longitudinal wave, it can transmit through liquid or solid bodies.

There is another kind of wave that can also occur in solid bodies, the transverse wave. Unlike the longitudinal wave, the direction of the vibration of the particles in transverse wave is perpendicular to the direction of propagation of the wave. An instantaneous picture of the particle motion of transverse wave is shown in Figure 2. It can be seen that in this case the particles oscillate at right angles or transverse to the direction of propagation and they oscillate sinusoidally up and down around their equilibrium positions.

A few parameters of a wave will be defined below. The frequency v is the number of waves passing through a given place within a certain period of time. The wavelength λ is the

displacement between two planes in which the particles are in the same state of motion. The relationship between wavelength and frequency can be obtained as follows:

$$\lambda = \frac{u}{v} \tag{2.1.1-1}$$

The common unit of propagation velocity u in the above equation is meter per second (m/s), the unit of frequency v is Hertz (Hz), and the unit of wavelength λ is meter (m).

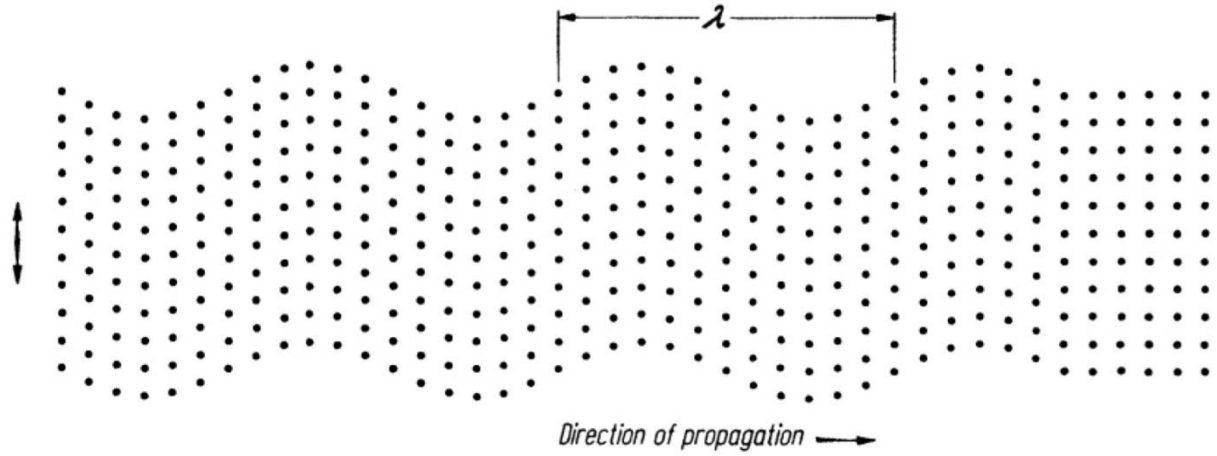

Figure 2. Transverse wave [9]

2.1.2 Rayleigh waves

There are three kinds of body waves in saturated soil: compression waves P_1 and P_2 and shear wave S. Rayleigh wave is a wave that travels near a solid surface, which is a surface wave generated by the interference of the P wave and the S wave due to the action of the free boundary. Rayleigh waves include longitudinal and lateral motion, and the amplitude decreases exponentially as the distance from the surface increases. Near the surface, the trajectory of the

particle is an ellipse. They can be produced in materials in a variety of ways, such as by local impact or by piezoelectric transformation.

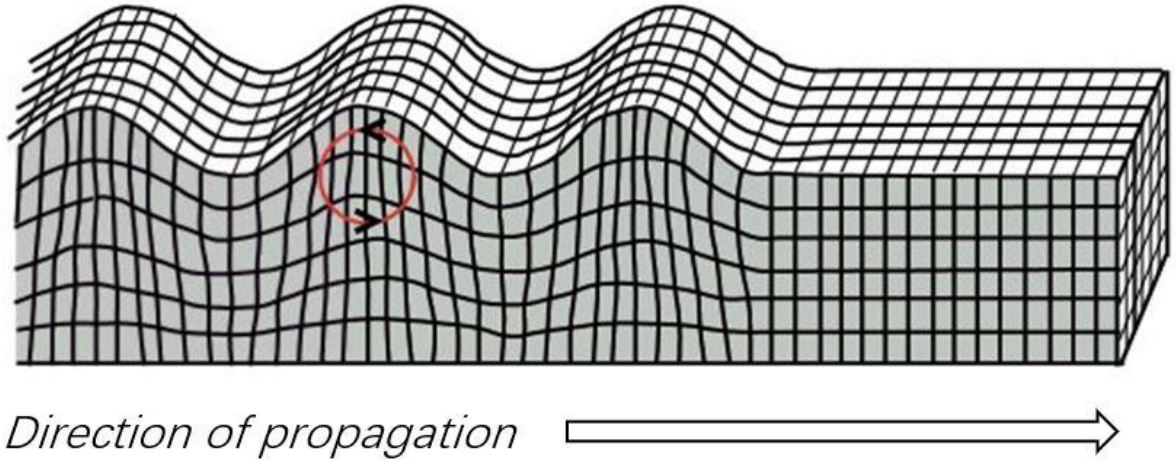

Figure 3. Rayleigh wave [10]

The existence of Rayleigh wave and its propagation properties were first revealed in 1885 by Lord Rayleigh, after whom they were named. In seismology, Rayleigh wave is part of the seismic waves generated by earthquakes. At a distance from the wave source, its destructive power is much larger than the longitudinal and transverse waves that extend in all directions along the space. Therefore, Rayleigh wave is one of the main research objects in seismology and can be used for geological exploration. Rayleigh waves are very sensitive to surface defects and other surface features and they propagate along the surface around curves. Because of this, Rayleigh waves are widely used in non-destructive material characterization to discover the mechanical and structural properties of the object being tested, such as the presence of cracks and associated shear modulus and can be used to inspect areas where other waves might be hard to reach.

2.2 ELASTIC WAVES IN SOLIDS

2.2.1 Elastic constants for isotropic materials

Consider a stressed small volume of crystal which has the original shape of cube. Choose the Cartesian coordinate system with three orthonormal axes x_1, x_2 and x_3 as the reference system, parallel to the cube's sides, as shown in Figure 4.

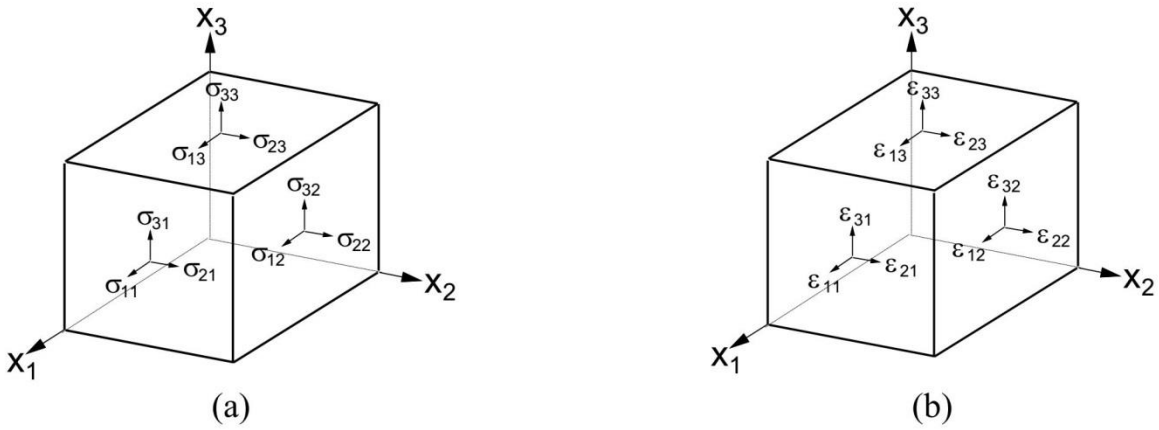

Figure 4. (a) Stress notation; (b) Strain notation [11]

Stresses σ and Strains ε are identified by two subscripts: i and j for stresses σ, and k and l for strains ε. Each of these subscripts counts from 1 to 3. For stresses, subscript i denotes the axial direction x_i of the stress component that transmitted along the cube surface and subscript j denotes the axial direction x_j of the normal of this surface. Similarly, for strains, subscript k denotes the axial direction x_k of the strain and subscript l denotes the axial direction x_l of the tensile force [12].

Elastic materials can be characterized by a relation between stresses and strains. For linear elastic materials, this relation can be represented by the Hooke's Law:

$$\sigma = c\varepsilon \tag{2.2.1-1}$$

In three dimensions, a generalized Hooke's Law in the form of a fourth-order tensor is:

$$\sigma_{ij} = \sum_{kl} c_{ijkl}\, \varepsilon_{kl} \tag{2.2.1-2}$$

in which the σ_{ij} is the second-rank stress tensor, the ε_{kl} is the second-rank strain tensor and the fourth-rank coefficients c_{ijkl} are called the elastic constants. Each of the indices ijkl is an integer from 1 to 3, thus there are 81 of the c_{ijkl}. Conversely, the stress tensor σ_{kl} is related to the strain tensor ε_{ij} by relation [13]:

$$\varepsilon_{ij} = \sum_{kl} s_{ijkl}\, \sigma_{kl} \tag{2.2.1-3}$$

Where the coefficients s_{ijkl} are called the compliance constants.

There are many symmetry relations among the tensors, so we can make a considerable reduction to the tensors with some simplified notations. The most well-known matrix formalisms for elasticity is that of Voigt, the stress and strain tensors are written as follows:

$$c_{ijkl} = c_{ijlk} = c_{jikl} \tag{2.2.1-4}$$

$$\sigma_{ij} = \sigma_{ji} \tag{2.2.1-5}$$

$$\varepsilon_{kl} = \varepsilon_{lk} \tag{2.2.1-6}$$

Thus, the number of elastic constants reduces from 81 to 36. According to the Voigt Notation, the matrix form of the Hooke's law becomes [14]:

$$\begin{Bmatrix} \sigma_1 \\ \sigma_2 \\ \sigma_3 \\ \sigma_4 \\ \sigma_5 \\ \sigma_6 \end{Bmatrix} = \begin{bmatrix} c_{11} & c_{12} & c_{13} & c_{14} & c_{15} & c_{16} \\ c_{21} & c_{22} & c_{23} & c_{24} & c_{25} & c_{26} \\ c_{31} & c_{32} & c_{33} & c_{34} & c_{35} & c_{36} \\ c_{41} & c_{42} & c_{43} & c_{44} & c_{45} & c_{46} \\ c_{51} & c_{52} & c_{53} & c_{54} & c_{55} & c_{56} \\ c_{61} & c_{62} & c_{63} & c_{64} & c_{65} & c_{66} \end{bmatrix} \begin{Bmatrix} \varepsilon_1 \\ \varepsilon_2 \\ \varepsilon_3 \\ \varepsilon_4 \\ \varepsilon_5 \\ \varepsilon_6 \end{Bmatrix} \tag{2.2.1-7}$$

Thermodynamic arguments can further reduce the number of elastic constants, which is reduced from 36 to 21 due to the symmetry about ij and kl: $c_{ijkl} = c_{klij}$, or in the reduced notation, $c_{mn} = c_{nm}$. Then Equation (2.2.1-6) becomes

$$\begin{Bmatrix}\sigma_1\\ \sigma_2\\ \sigma_3\\ \sigma_4\\ \sigma_5\\ \sigma_6\end{Bmatrix} = \begin{bmatrix}c_{11} & c_{12} & c_{13} & c_{14} & c_{15} & c_{16}\\ c_{12} & c_{22} & c_{23} & c_{24} & c_{25} & c_{26}\\ c_{13} & c_{23} & c_{33} & c_{34} & c_{35} & c_{36}\\ c_{14} & c_{24} & c_{34} & c_{44} & c_{45} & c_{46}\\ c_{15} & c_{25} & c_{35} & c_{45} & c_{55} & c_{56}\\ c_{16} & c_{26} & c_{36} & c_{46} & c_{56} & c_{66}\end{bmatrix} \begin{Bmatrix}\varepsilon_1\\ \varepsilon_2\\ \varepsilon_3\\ \varepsilon_4\\ \varepsilon_5\\ \varepsilon_6\end{Bmatrix} \tag{2.2.1-8}$$

Thus, as well known, this is the general form of the elastic constant matrix with 21 independent components. A crystal that has this form of elastic constant matrix is called a triclinic body. It has no material symmetries so the number of independent elastic components cannot be reduced, which remains 21. Considering the symmetry conditions found in different crystal structures, the 21 independent elastic constants can be reduced further.

For the monoclinic bodies, the only symmetry of it is a reflection in a plane about a single axis, called an axis of two-fold symmetry. Suppose $x_3 = 0$ is the symmetry plane, we get

$$c_{14} = c_{24} = c_{34} = c_{15} = c_{25} = c_{35} = c_{46} = c_{56} = 0 \tag{2.2.1-9}$$

Hence, a monoclinic body depends upon only 13 independent elastic constants and the elasticity matrix $[C]$ appears as

$$[C] = \begin{bmatrix}c_{11} & c_{12} & c_{13} & 0 & 0 & c_{16}\\ c_{12} & c_{22} & c_{23} & 0 & 0 & c_{26}\\ c_{13} & c_{23} & c_{33} & 0 & 0 & c_{36}\\ 0 & 0 & 0 & c_{44} & c_{45} & 0\\ 0 & 0 & 0 & c_{45} & c_{55} & 0\\ c_{16} & c_{26} & c_{36} & 0 & 0 & c_{66}\end{bmatrix} \tag{2.2.1-10}$$

For the orthotropic bodies, we should add another plane of symmetry orthogonal to the previous one, the plane $x_2 = 0$. So, this symmetry adds four supplementary conditions:

$$c_{16} = c_{26} = c_{36} = c_{45} = 0 \tag{2.2.1-11}$$

Since the existence of two orthogonal planes of elastic symmetry is physically impossible, in other words, only one or three mutually orthogonal planes of symmetry is admissible, we should add a third plane of symmetry, the plane $x_1 = 0$. However, this symmetry does not give any additional conditions to the elasticity matrix. A system having three planes of symmetry is called orthotropic system. Its elasticity matrix which depends upon 9 distinct elastic moduli looks as follows [15]:

$$[C] = \begin{bmatrix} c_{11} & c_{12} & c_{13} & 0 & 0 & 0 \\ c_{12} & c_{22} & c_{23} & 0 & 0 & 0 \\ c_{13} & c_{23} & c_{33} & 0 & 0 & 0 \\ 0 & 0 & 0 & c_{44} & 0 & 0 \\ 0 & 0 & 0 & 0 & c_{55} & 0 \\ 0 & 0 & 0 & 0 & 0 & c_{66} \end{bmatrix} \tag{2.2.1-12}$$

For cubic bodies, the x_i axes are all equivalent, we have

$$c_{11} = c_{22} = c_{33}, c_{44} = c_{55} = c_{66},\ c_{12} = c_{13} = c_{23} \tag{2.2.1-13}$$

Thus, there are three independent elastic constants in cubic elasticity matrix:

$$[C] = \begin{bmatrix} c_{11} & c_{12} & c_{12} & 0 & 0 & 0 \\ c_{12} & c_{11} & c_{12} & 0 & 0 & 0 \\ c_{12} & c_{12} & c_{11} & 0 & 0 & 0 \\ 0 & 0 & 0 & c_{44} & 0 & 0 \\ 0 & 0 & 0 & 0 & c_{44} & 0 \\ 0 & 0 & 0 & 0 & 0 & c_{44} \end{bmatrix} \tag{2.2.1-14}$$

In isotropic case, there exists a relationship:

$$c_{44} = \frac{1}{2}(c_{11} - c_{12}) \tag{2.2.1-15}$$

Thus, the isotropic case has two independent elastic constants.

2.2.2 Elastic constants and surface wave

Young's modulus, also known as tensile modulus, is the most common one of elastic modulus or modulus of elasticity. Young's modulus is a measure of the stiffness of an isotropic elastomer, defined as the ratio between uniaxial stress and uniaxial deformation within the range applicable to Hooke's law. Young's modulus can be expressed in terms of the elastic constants by

$$\mathrm{E} = \frac{c_{11}^2 + c_{11}c_{12} - 2c_{12}^2}{c_{11} + c_{12}} \tag{2.2.2-1}$$

The isotropic case is handled by substituting equation 2.2.1-15, we get

$$\mathrm{E} = c_{44}\frac{(3c_{11} - 4c_{44})}{c_{11} - c_{44}} \tag{2.2.2-2}$$

The speeds of longitudinal wave v_l and transverse wave v_t can also be expressed by elastic constants:

$$v_l = \sqrt{c_{11}/\rho} \tag{2.2.2-3}$$

$$v_t = \sqrt{c_{44}/\rho} \tag{2.2.2-4}$$

Where ρ is the density of solid.

By substituting equations 2.2.2-3 and 2.2.2-4 into equation 2.2.2-2, the Young's modulus for isotropic materials can be written as

$$\mathrm{E} = \rho v_t^2\frac{(3v_l^2 - 4v_t^2)}{v_l^2 - v_t^2} \tag{2.2.2-5}$$

Viktorov gave a relationship between the speeds of longitudinal wave v_l, transverse wave v_t and the speed of Rayleigh surface wave v_R [16, 17]:

$$v_R = v_t \frac{0.718 - \left(\frac{v_t}{v_l}\right)^2}{0.75 - \left(\frac{v_t}{v_l}\right)^2} \quad (2.2.2\text{-}6)$$

We can calculate the speed of longitudinal wave v_l and the speed of Rayleigh surface wave v_R through measurement and the transverse wave velocity v_t can be calculated by solving equation 2.2.2-6.

2.3 EXPERIMENTAL METHOD

2.3.1 Snell's law and incident angle

2.3.1.1 Snell's law

When light waves propagate from one medium to another medium with a different refractive index, refraction occurs, and the relationship between the angle of incidence and the angle of refraction can be described by Snell's Law, as shown in the following equation:

$$\frac{\sin\theta_1}{\sin\theta_2} = \frac{v_1}{v_2} \quad (2.3.1\text{-}1)$$

Where θ_1 is the angle between the incident light and the interface normal; θ_2 is the angle between the refracted light and the interface normal; v is the velocity of light in the respective medium.

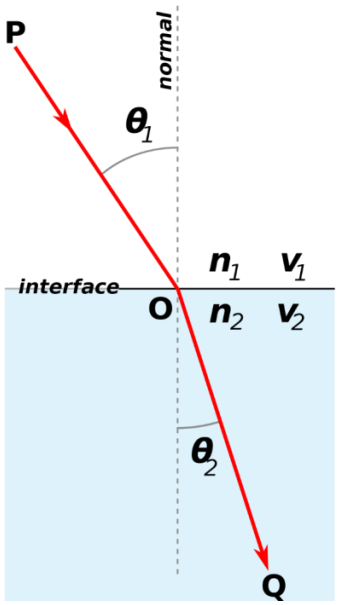

Figure 5. Refraction and reflection of light [18]

Unlike the reflection of light, when acoustic wave travels in a solid material, one form of wave energy can be transformed into another form. In other words, when a longitudinal wave hits an interface at an angle, some of the energy can cause particle movement in the transverse direction and produce a transverse (shear) wave. At this time, the relationship between the transverse wave reflection angle and the longitudinal wave incident angle is the same as described in the Snell's law of light:

$$\frac{\sin\theta_1}{v_{L_1}} = \frac{\sin\theta_2}{v_{L_2}} = \frac{\sin\theta_3}{v_{S_1}} = \frac{\sin\theta_4}{v_{S_2}} \qquad (2.3.1\text{-}2)$$

Where θ_1 is the angle between the incident longitudinal wave (or reflected longitudinal wave) and the interface normal; θ_2 is the angle between the refracted longitudinal wave and the interface normal; θ_3 is the angle between the reflected shear wave and the interface normal; θ_4 is the angle between the refracted shear wave and the interface normal; v_L and v_S are the velocities of longitudinal wave and shear wave in the respective medium.

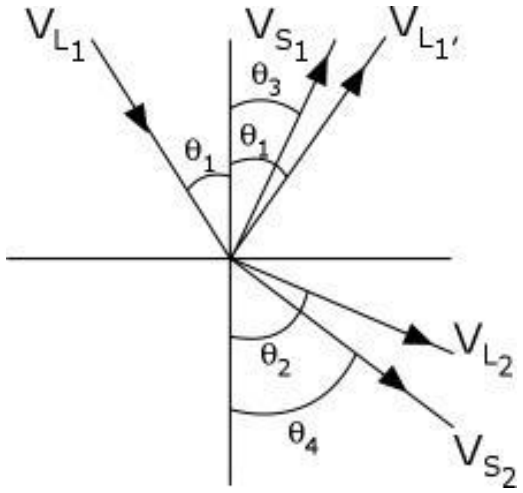

Figure 6. Refraction and reflection of acoustic wave [19]

2.3.1.2 First critical angle

When the wave moves from a medium with a higher refractive index to a medium of lower refractive index, the angle of refraction will be greater than the angle of incidence. When the angle of incidence is a certain value, the angle of refraction is equal to 90°, and the angle of incidence is called the first critical angle. When the longitudinal wave incident angle is greater than the first critical angle, there is no longer a refracting longitudinal wave in the second medium, only the refracting transverse wave.

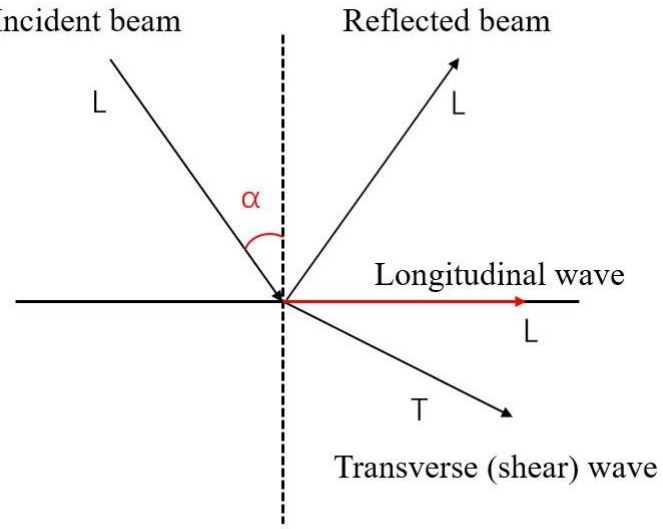

Figure 7. First critical angle

2.3.1.3 Second critical angle

When the longitudinal wave incident angle continues to increase beyond the first critical angle, the transverse wave refraction angle in the second medium also increases. There is an incident angle that makes the transverse angle of refraction 90 degrees and is known as the second critical angle. At this point, there is no wave in the second medium and all the wave energy is reflected or refracted into the surface. Thus, surface waves (Rayleigh waves) will be generated slightly beyond the second critical angle.

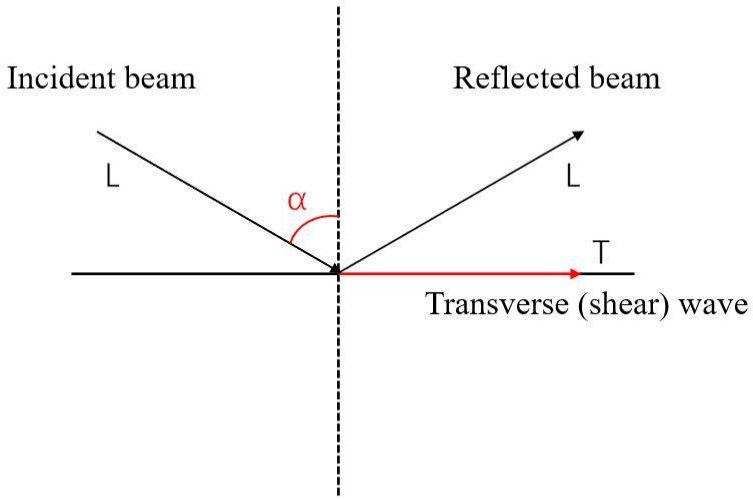

Figure 8. Second critical angle

2.4 CORROSION MECHANISM

Metal corrosion is generally defined as metamorphism and destruction caused by chemical and electrochemical interactions between the metal and the surrounding medium. Corrosion of carbon steel in the atmosphere, corrosion of steel in seawater, perforation of underground pipelines in the soil, damage of boilers in thermal power plants, and damage to metal machinery and equipment caused by contact with corrosive media (acids, bases and salts) are the most common corrosion phenomena. Obviously, metal corrosion requires an external environment. Chemical or electrochemical heterogeneous reactions occur at the metal surface or interface, converting the metal to an oxidized (ion) state. Therefore, the chemical and electrochemical reactions occurring in the corrosion system formed by metals and the environment are the main research contents of metal corrosion.

In seawater submerged zone, corrosion is dominated by electrochemical corrosion. Electrochemical corrosion refers to the damage caused by the electrochemical reaction between the metal surface and the ion-conducting medium. An electric current is generated during the reaction, and a cathode and an anode exist on the surface of the corroded metal. The anodic reaction is a process in which a metal atom loses electrons and becomes an ionic state and is transferred to a medium, which is called an anodization process. The cathodic reaction is the removal of electrons from the anode by a depolarizer in the medium, known as the cathodic reduction process. These two reactions are carried out independently of each other and are referred to as a pair of conjugation reactions. The chemical equations of the corrosion process at the anode is [20]:

$$Me \rightarrow Me^{n+} + \mathrm{n}e^{-} \tag{2.4-1}$$

The chemical reaction equation at the cathode is:

$$O_2 + 2H_2O + 4e^{-} \rightarrow 4OH^{-} \tag{2.4-2}$$

The characteristics of seawater corrosion are also related to chloride ions (Cl^{-}). The salinity of seawater is about 3.2-3.7 wt%, which can be regarded as a 3.5 wt% sodium chloride (NaCl) solution. Chloride ions are reactive anions that can cause partial damage to the passivation film of the metals. So far, the mechanism of how chloride ions convert the passivated metal into an activated state is still inconclusive, but it can be roughly divided into two viewpoints.

One is called the oxide-film theory. According to this theory, when the metal is dissolved, a dense, well-covered protective film can be formed on the surface. This protective film exists as a separate phase and mechanically separates the metal from the solution, thereby greatly reducing the rate of metal dissolution and even turning the metal into a passive state. Protective

film is usually a metal oxide. The chloride ion has a small radius and a strong penetrating ability, so it can easily penetrate the small gap in the oxide film to reach the metal surface and interacts with the metal to form a soluble compound, which changes the structure of the oxide film.

The other one is called the adsorption theory. According to this theory, metal passivation is due to the formation of oxygen or oxygen-containing adsorption layers on the metal surface, which changes the structure of the metal/solution interface and makes the activation energy of the anode reaction significantly increase and passivation occurs. Since chloride ions have a strong ability to be adsorbed by metals, they are preferentially adsorbed by metals and ventilate oxygen from the metal surface. Chloride ions form chlorides which are soluble with metals, causing the acceleration of corrosion.

3.0 EXPERIMENTAL DESIGN

3.1 Design and manufacture of line-focus transducer

3.1.1 Design of line-focus transducer

As mentioned before, Rayleigh wave velocity is extremely useful in material characterization. Based on the ray representation of converging beam and reflected waves, Yamanaka developed an absolute velocity measurement method of leaky surface wave using a broadband impulsive converging beam.

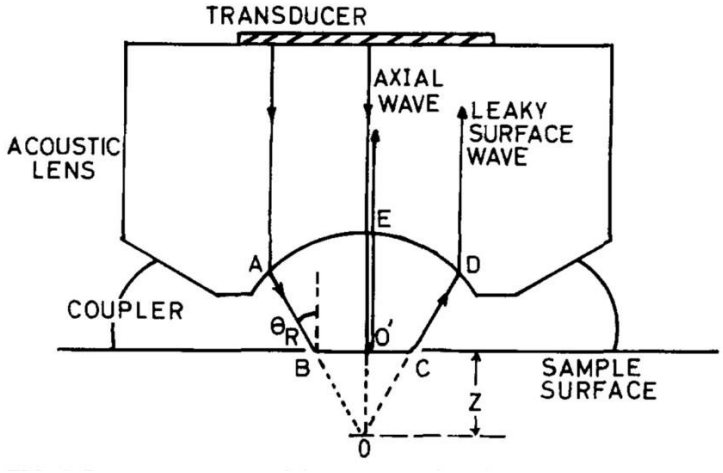

Figure 9. Ray representation of wave propagation [21]

As shown in Figure 9, is the transducer and ray components analyzed by Yamanaka [21]. The axial wave emitted by acoustic lens is reflected by the sample surface and follows the path EO'E. An obliquely incident ray component incidents at Rayleigh critical angle θ_R and excites

the Rayleigh surface wave on the sample surface. It travels along the surface for a distance before goes back to the lens and follows the path ABO'CD.

In this paper, the line-focus transducer is designed refer to the design of Xiang D. as shown in Figure 10.

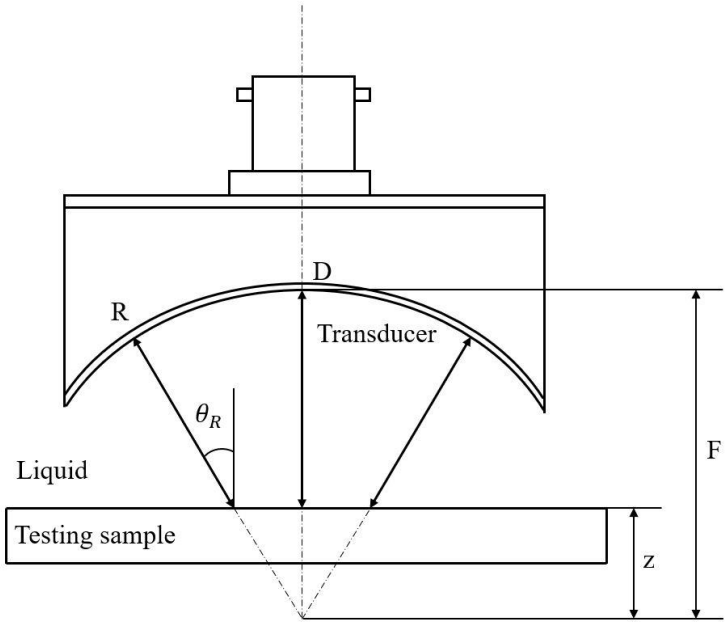

Figure 10. Schematic of line-focus transducer

Based on the wave propagation path in Figure 10, the traveling time of the directly reflected wave from the sample surface is

$$t_1 = \frac{2(F - z)}{v_w} \tag{3.1.1-1}$$

Where F is the distance between the midpoint of the acoustic lens and the focal point, z is the defocal distance between the sample surface and the focal plane, v_w is the longitudinal wave velocity of the coupling medium (which is distilled water in this paper, $v_w = 1482\ m/s$).

The traveling time of the Rayleigh surface wave is

$$t_2 = \frac{2(F - \frac{z}{\cos\theta_R})}{v_w} + \frac{2z\tan\theta_R}{v_R} \tag{3.1.1-2}$$

Where θ_R is the Rayleigh wave critical angle, and v_R is the velocity of the Rayleigh surface wave.

According to Snell's law,

$$\frac{v_w}{v_R} = \frac{\sin\theta_R}{\sin 90°} \tag{3.1.1-3}$$

From equations 3.1.1-1, 3.1.1-2, and 3.1.1-3 the time interval between the directly reflected wave and the Rayleigh surface wave is

$$t = t_2 - t_1 = \frac{2(1-\cos\theta_R)}{v_w} z \tag{3.1.1-4}$$

Equation 3.1.1-4 shows that the time interval we derived above is linear with the defocus distance z, this relationship can be represented as

$$\frac{dz}{dt} = \frac{v_w}{2(1-\cos\theta_R)} \tag{3.1.1-5}$$

From equation 3.1.1-3 and 3.1.1-5 the Rayleigh surface wave velocity can be expressed as

$$v_R = \left[\frac{1}{v_w(\frac{dz}{dt})} - \frac{1}{4(\frac{dz}{dt})^2}\right]^{-\frac{1}{2}} \tag{3.1.1-6}$$

Also, the longitudinal wave velocity can be calculated by

$$v_L = \frac{2d}{t_L} \tag{3.1.1-7}$$

Where d is the thickness of the testing sample and t_L is the traveling time of the longitudinal wave in the sample [22, 23].

3.1.2 Manufacture of line-focus transducer

Polyvinylidene difluoride (PVDF) is a highly non-reactive semi-crystalline polymer which is widely used in aerospace, railway, petrochemical and other modern industrial fields. PVDF piezoelectric film has good mechanical and piezoelectric properties and is suitable for making acoustic wave receiving devices. Commercial PVDF film has the advantages of flexibility and low acoustic impedance. The thickness of the PVDF film is extremely thin and can be closely attached to the surface of the object with an arbitrary arc. Its low acoustic impedance can provide good match with the backing material and coupling liquid [24].

An aluminum rectangular tube (fabricated by McMASTER-CARR) with required curvature at one end and flat at the other end was used as the case of the transducer. Epoxy (Devcon, No.14310) was mixed with tungsten powder (Alfa Aesar, -325 mesh, 99.9%, metal basis) at a weight ratio of 1:2 as the backing material. Here an aluminum tube was used as mandrel as shown in Figure 11.

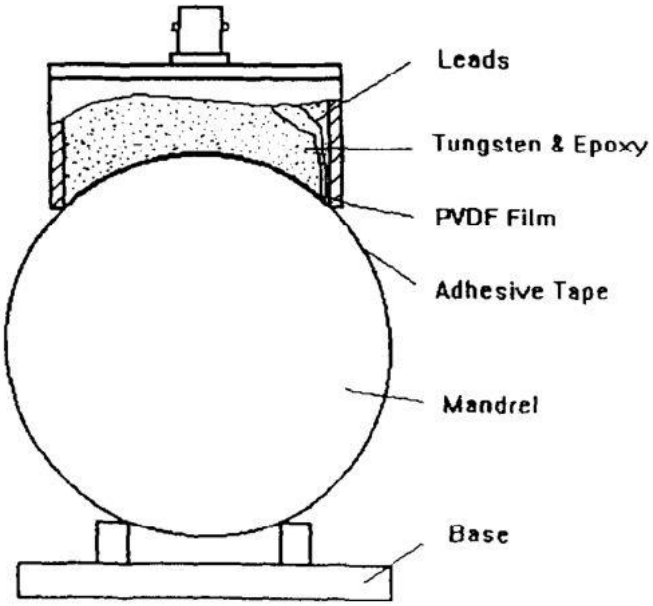

Figure 11. Transducer fabrication procedure [5]

A rectangular PVDF film (DT-028, NEG, 60 mm ∗ 12.5 mm, thickness 30 um) was affixed to the surface of the mandrel with adhesive tape in advance. After standing overnight, the transducer was taken down and the leads part was covered with hot glue to make sure it is waterproof. The final product is shown in Figure 12.

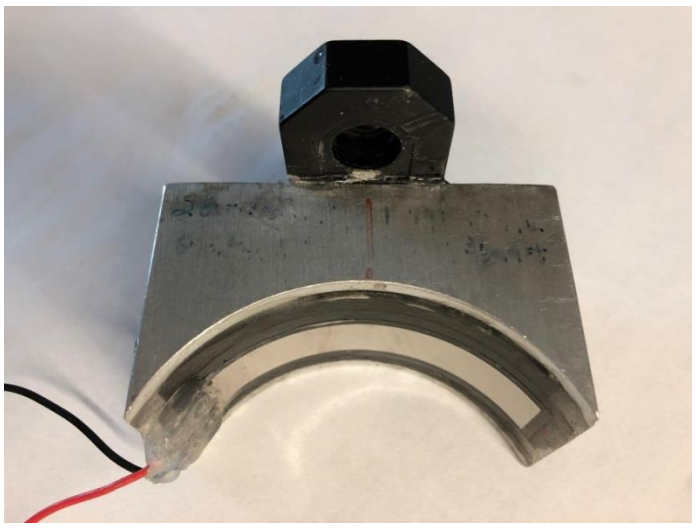

Figure 12. Line-focus PVDF transducer

3.2 System setup

The measurement system we adopt here is the same one in Chenglong's work [25]. The line-focus ultrasonic measurement system includes a line-focus PVDF transducer mentioned above, an oscilloscope (4034A, Agilent Technologies), a manually controlled ultrasonic pulser/receiver (5072PR, OLYMPUS), motorized stages, a stage controller (SURUGA SEIKI CO., LTD), and a computer. The schematic of the system is shown in Figure 13.

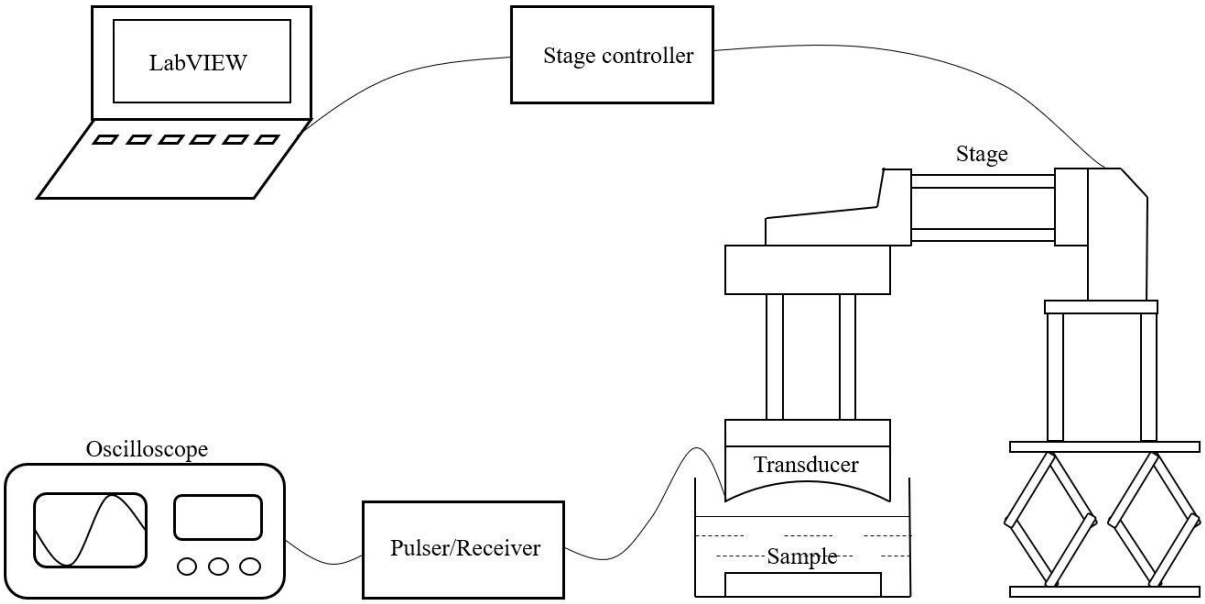

Figure 13. Schematic of system setup

When the pulser/receiver generates a pulse, the transducer is excited and generates acoustic waves which will incident on the surface of the sample. Then the reflected wave will be received by the receiver and converted into electrical signal. The signal can be observed by the oscilloscope in the form of a waveform. A LabVIEW program is used to give instructions to the

stage controller to control the movement of the stages, thereby enabling the control of the position of the transducer. The actual setup of the equipment is shown in Figure 14.

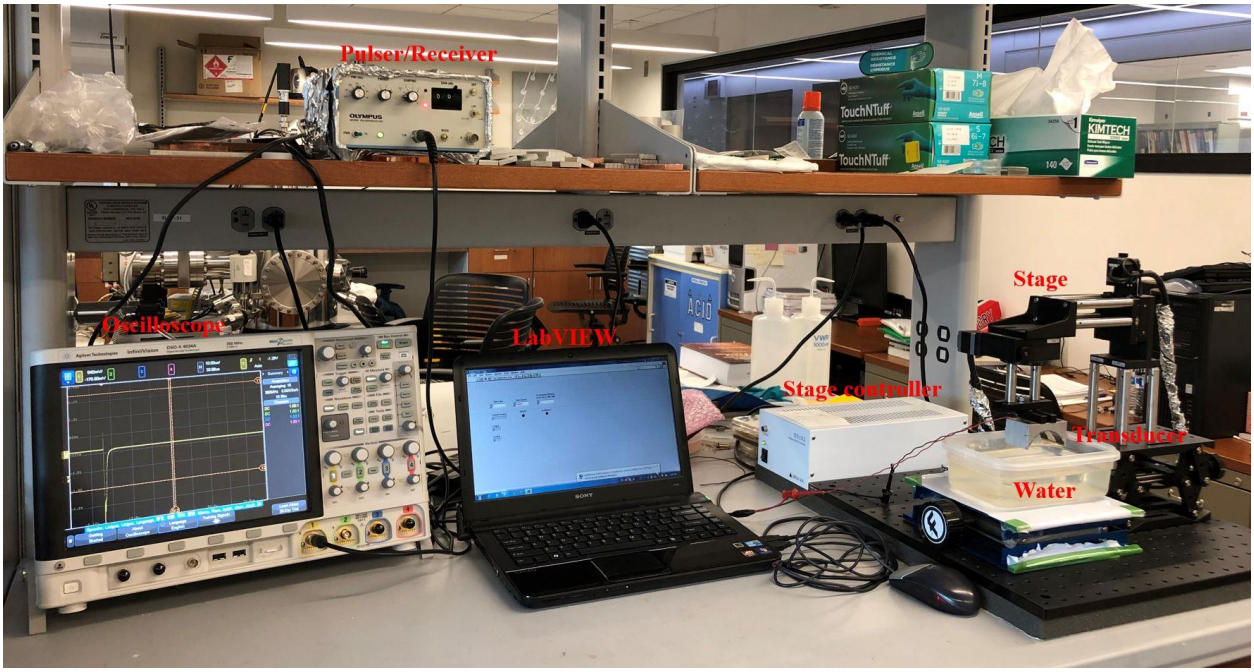

Figure 14. System setup

3.3 Sample corrosion

We selected four metal alloys commonly used in industrial fields: 304 stainless steel, low-carbon steel, 6061 aluminum and multipurpose 110 copper (McMASTER-CARR) as the research sample. The basic properties and chemical composition of these materials are shown in Table 1-3.

Table 1. Composition sheet of 304 stainless steel

Element	Content (%)
Carbon	0.08
Iron	65.8-70.8
Manganese	2.00
Phosphorus	0.045
Sulfur	0.030
Silicon	1.00
Chromium	18.0-20.0
Nickel	8.0-11.0

Table 2. Composition sheet of Low-carbon steel

Element	Content (%)
Carbon	0.17-0.230
Iron	99.08-99.53
Manganese	0.30-0.60
Phosphorous	$\leq$ 0.040
Sulfur	$\leq$ 0.050

Table 3. Composition sheet of 6061 aluminum

Element	Content (%)
Aluminum	96-97.36
Silicon	0.40-0.8
Iron	0.7
Copper	0.15-0.40
Manganese	0.15
Magnesium	0.8-1.2
Chromium	0.04-0.35
Zinc	0.25
Titanium	0.15

Multipurpose 110 copper contains a minimum proportion of copper of 99.9 % and the proportion of other elements is negligible.

The specimens were corroded through submersion in a 3.5% (wt%) NaCl solution. To accelerate the corrosion procedure, sulfuric acid with a concentration of 0.05 mol/L was added and air was pumped into the solution. The corrosion procedure is shown in Figure 15, taking the corrosion of multipurpose 110 copper as an example.

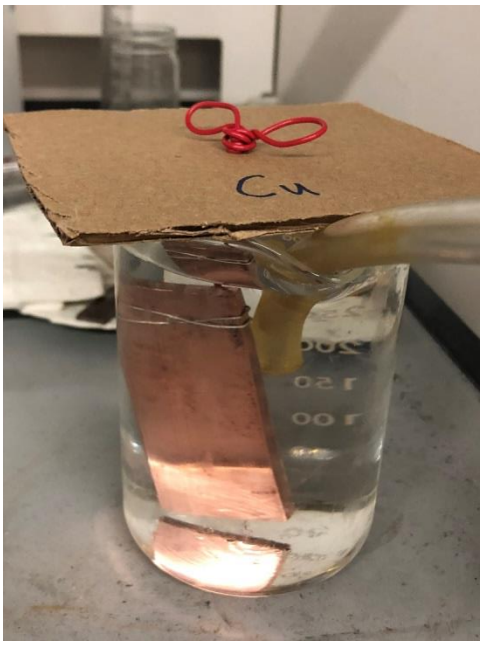

Figure 15. Corrosion procedure

The corrosion time was set to 5, 10, 15, 20, 25 days respectively. The corrosion solution was replaced after each measurement. After corrosion, the properties of the sample surfaces were changed.

After 5 days of corrosion, the surface of 6061 aluminum sample was covered with a thin, relatively dense white corrosion product which should be alumina (Al_2O_3) with the same white color. As time goes on, the corrosion product layer is continuously thickened. After 25 days of corrosion, there are loose and blocky white powdery corrosion products on the sample surface. After cleaning, many small pits were observed in the sample surface.

After corrosion, the surface of the multipurpose 110 copper sample was covered by a layer of green corrosion products which should be verdigris with a main component of $Cu_2(OH)_2CO_3$. This layer of corrosion products is relatively loose and very easy to break off. After cleaning, the surface darkened from the original red-orange with metallic luster to brown-

orange matte powder. This brown-orange product should be the mixture of copper oxide (CuO) and cuprous oxide (Cu_2O).

The surface of the 304 stainless steel sample was slightly darkened.

The low-carbon steel sample was coated by a reddish-brown rust layer whose main components were $FeOOH$ (iron oxide yellow), Fe_2O_3 (iron oxide red) and a small amount of Fe_3O_4 (iron oxide black). In order to further observe the corrosion behavior of the underlying metals, the rust layer was washed away from the sample surface and the sample was rinsed with distilled water. The underlying surface turned black after corrosion as shown in Figure 17 (d) and its main component was Fe_3O_4.

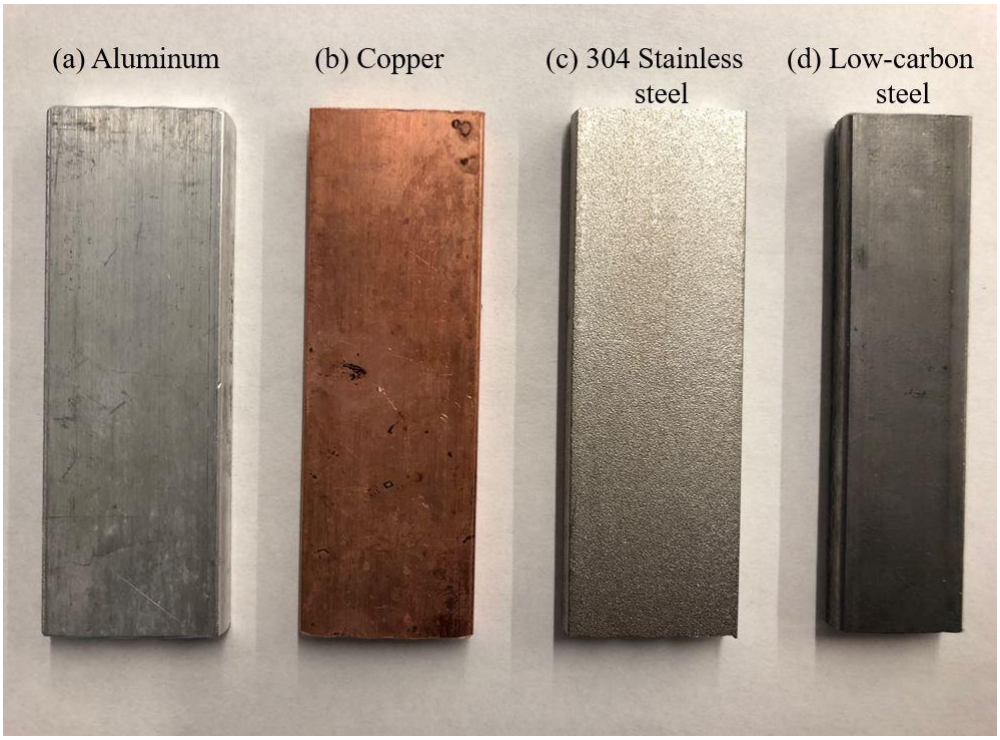

Figure 16. Samples before corrosion

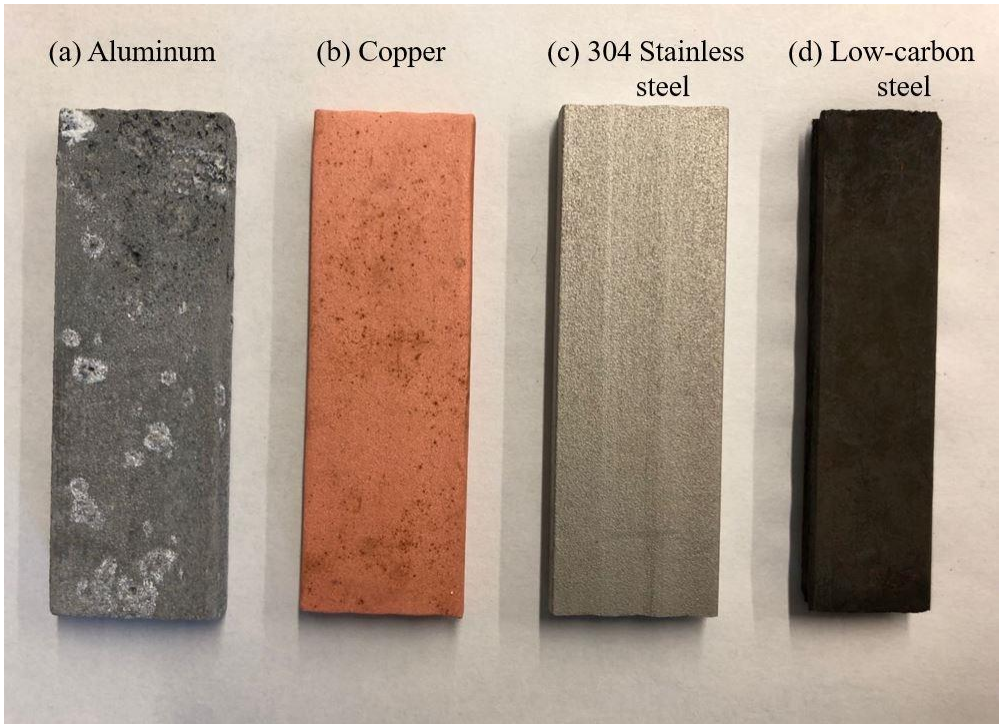

Figure 17. Corroded samples for 25 days after cleaning

The densities of the samples ρ were determined by measurement of mass m and volume V using equation

$$\rho = \frac{m}{V} \tag{3.3-1}$$

The mass m was measured using a pan balance and the volume V was measured using a graduated cylinder. Pour water into a graduated cylinder until it reaches a known level. Add the sample into the cylinder and record the new water level. The difference between the new water level and the original level is the volume of the sample.

3.4 Velocity measurement

First, we adjusted the sample to the focal position of the transducer, that is, adjust to the position where the received waveform reflected form the sample top surface had maximum amplitude. The waveform at the focal position is shown in Figure 18. The highest crest represents the peak of directed reflected wave from sample top surface which has high energy concentration. The last tiny crest represents the wave reflected from the sample bottom surface which is not obvious due to energy loss during wave propagation.

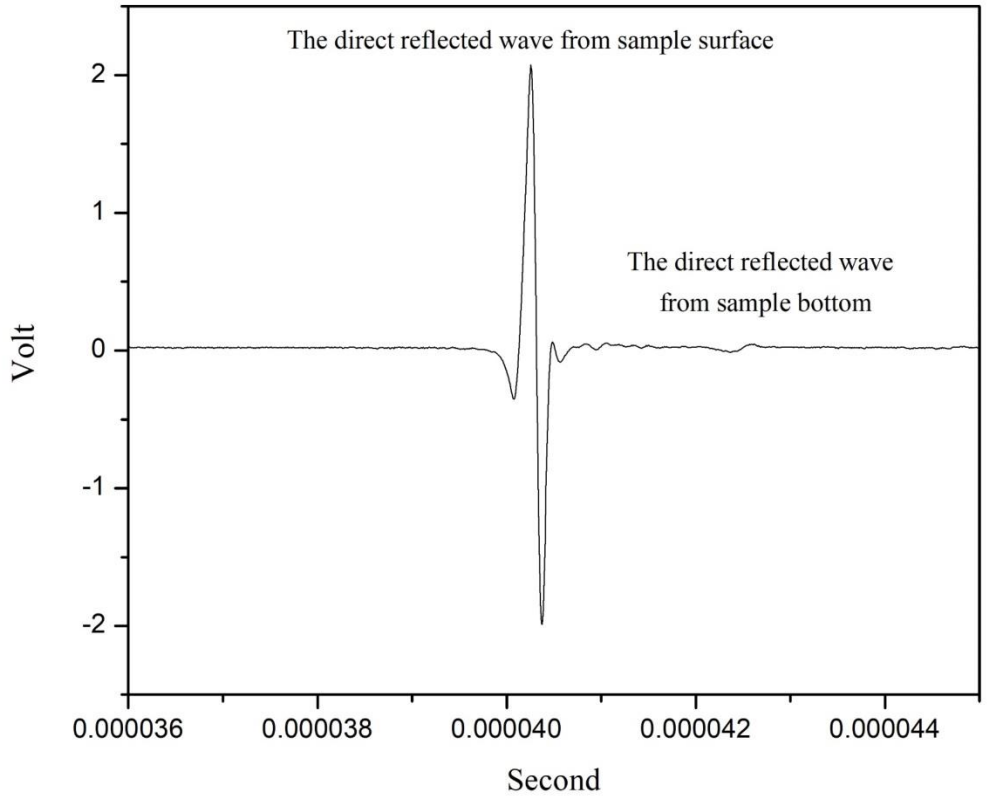

Figure 18. Waveform at focal position

Then lowered the transducer 0.2 mm each step for 10-15 times. As the transducer gradually approached the surface of the sample, the waves began to be separated and the Rayleigh surface wave could be found as shown in Figure 19. The required data was collected during the defocusing process: the time interval between the peak of direct reflected wave and the peak of Rayleigh surface wave; the time interval between the peak of direct reflected wave form sample top surface and the peak of the wave reflected from the sample bottom surface.

Finally, the data was collected and plotted, and the slope $\frac{dz}{dt}$ （the slope of the defocus position z versus the time interval between the directly reflected wave and the Rayleigh surface wave）was derived.

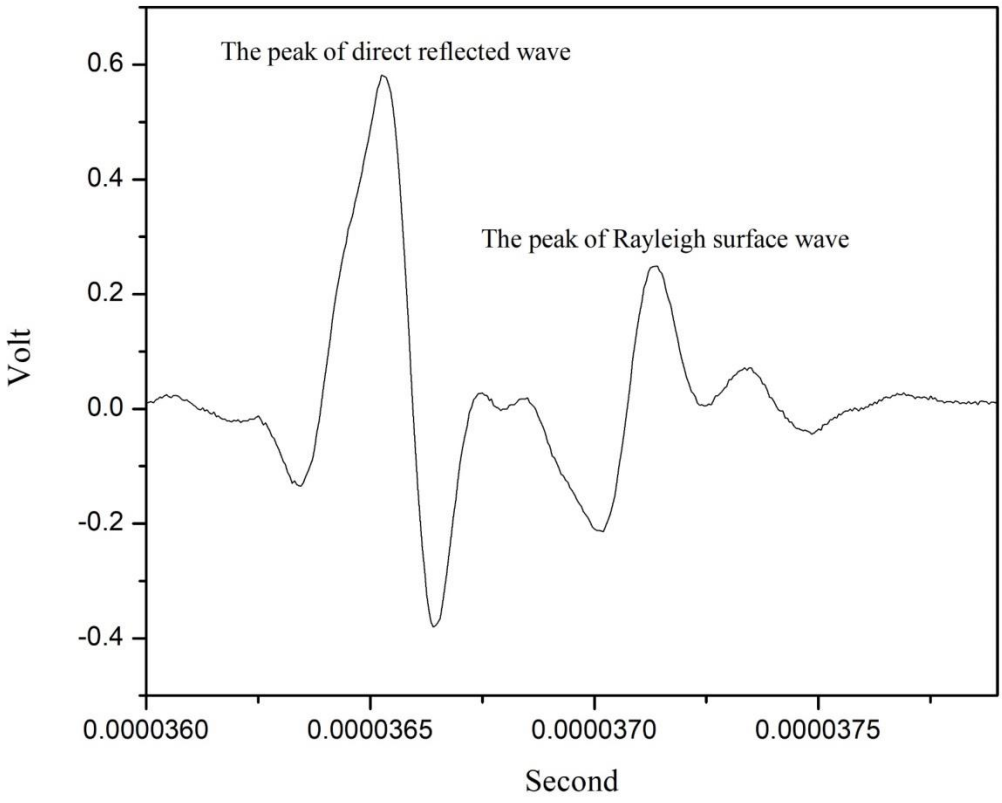

Figure 19. Waveform at defocus position

4.0 RESULTS AND DISCUSSIONS

In experiments, four common metal alloys, 304 stainless steel, low-carbon steel, 6061 aluminum and multipurpose 110 copper fabricated by McMASTER-CARR were tested. Set the focal position of the transducer as the original position. Plot the defocus position z (on the ordinate) versus the time interval between the directly reflected wave and the Rayleigh surface wave (on the abscissa). The slope $\frac{dz}{dt}$ was obtained by linearly fitting the coordinate points. All the results were obtain under room temperature (25℃).

4.1 304 stainless steel sample

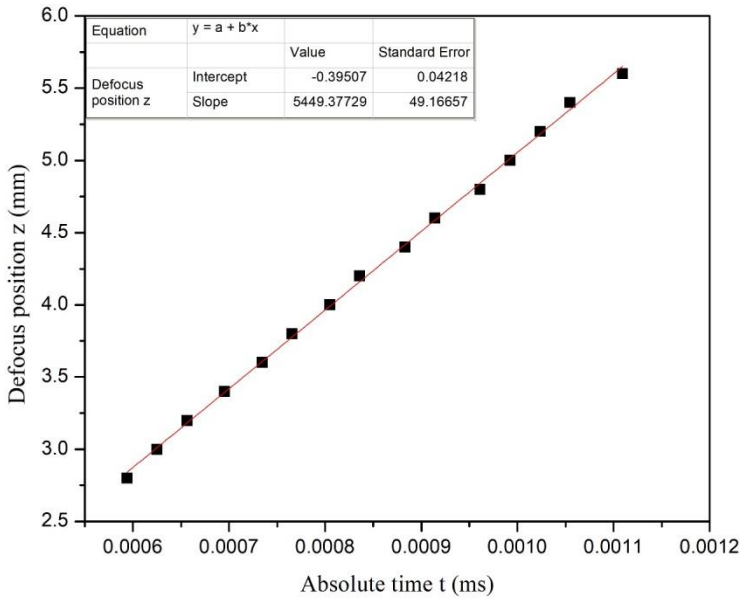

Figure 20. Defocus position vs. absolute time for the uncorroded 304 stainless steel

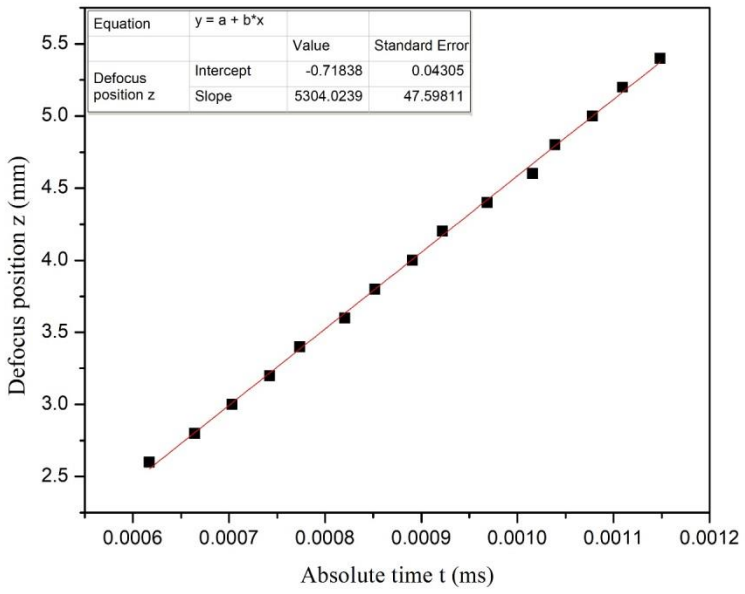

Figure 21. Defocus position vs. absolute time for the corroded 304 stainless steel (5-d)

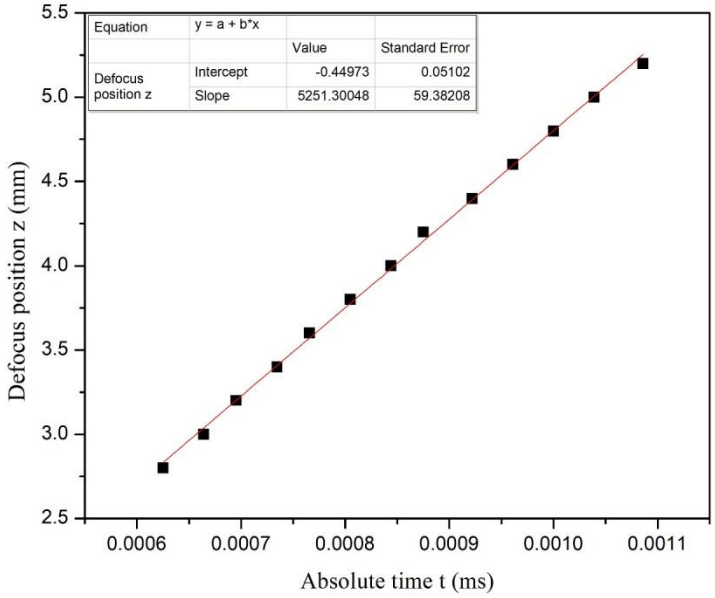

Figure 22. Defocus position vs. absolute time for the corroded 304 stainless steel (10-d)

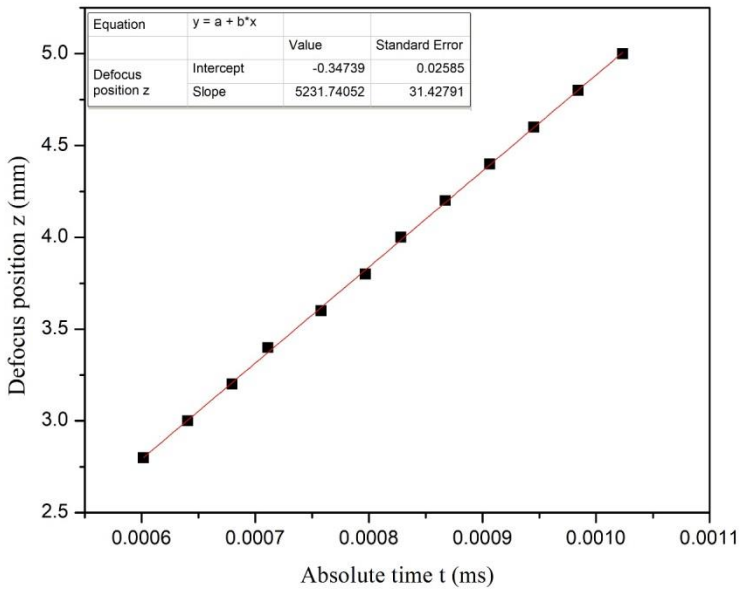

Figure 23. Defocus position vs. absolute time for the corroded 304 stainless steel (15-d)

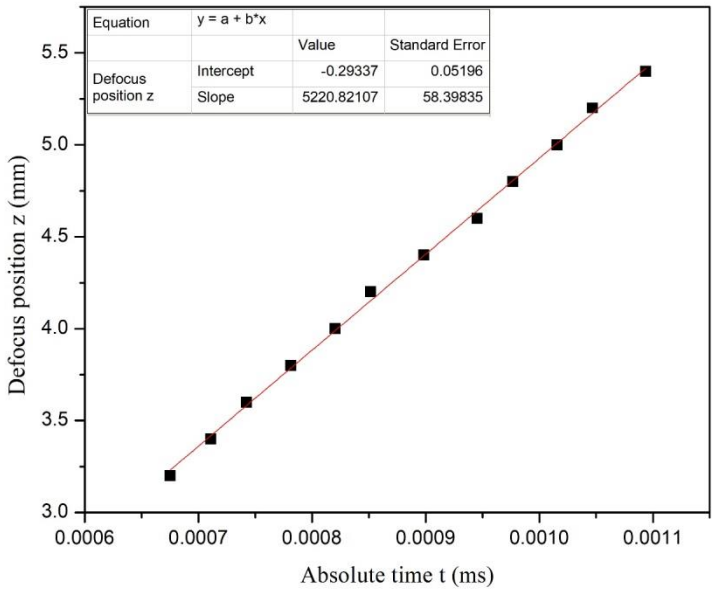

Figure 24. Defocus position vs. absolute time for the corroded 304 stainless steel (20-d)

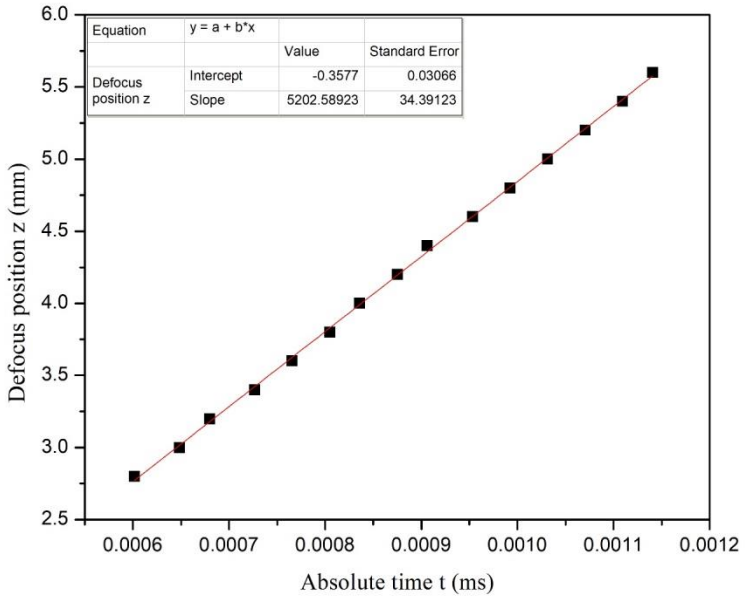

Figure 25. Defocus position vs. absolute time for the corroded 304 stainless steel (25-d)

As shown in the figures above, we have already got the values of $\frac{dz}{dt}$ for samples with different corrosion times, so we can calculate the velocities of the Rayleigh surface waves v_R by equation 3.1.1-6. The longitudinal wave velocities v_l can be calculated by equation 3.1.1-7. After getting v_R and v_l, we can get the transverse wave velocities v_t by solving equation 2.2.2-6. This equation has three roots. One of the roots is negative and very easy to exclude. The desired root can be chosen by an approximate formula [26]:

$$c_R \approx c_t(0.87 + 1.12v)(1 + v)^{-1} \qquad (4.1\text{-}1)$$

Where v is the Poisson ratio. Poisson's ratio is the ratio of the transverse positive strain to the absolute value of the axial positive strain when the material is subjected to tension or compression in one direction. For most materials, Poisson's ratio varies from 0 to 0.5, thus according to equation 4.1-1, c_R varies from $0.87c_t$ to $0.953c_t$.

The densities of the samples ρ were determined by measuring mass m and volume V using equation 3.3-1.

Based on the above data, the Young's modulus E was calculated by equation 2.2.2-5 and all data are summarized in Table 4.

Table 4. Summary of $\frac{dz}{dt}$, v_R, v_l, v_t and E of 304 stainless steel sample

Corrosion time (d)	$\frac{dz}{dt}$ (m/s)	v_R (m/s)	v_l (m/s)	v_t (m/s)	E (GPa) calculated	E (GPa) standard
0	5449.38	2943.66	5601.43	3181.95	201.87	193-200
5	5304.02	2907.04	5510.53	3144.07	199.84	-
10	5251.30	2893.65	5411.49	3135.93	196.95	-
15	5231.74	2888.66	5404.26	3130.33	196.05	-
20	5220.82	2885.88	5364.99	3130.50	194.81	-
25	5202.59	2881.22	5361.41	3124.96	194.06	-

As can be seen from Table 4, the velocity of the Rayleigh surface wave v_R decreases as the corrosion time increases. The calculated Young's modulus of the uncorroded 304 stainless steel sample is close to the standard value and it also decreases as the corrosion becomes severer.

The process of rust formation of steel in a chloride-containing environment can be represented by Figure 26:

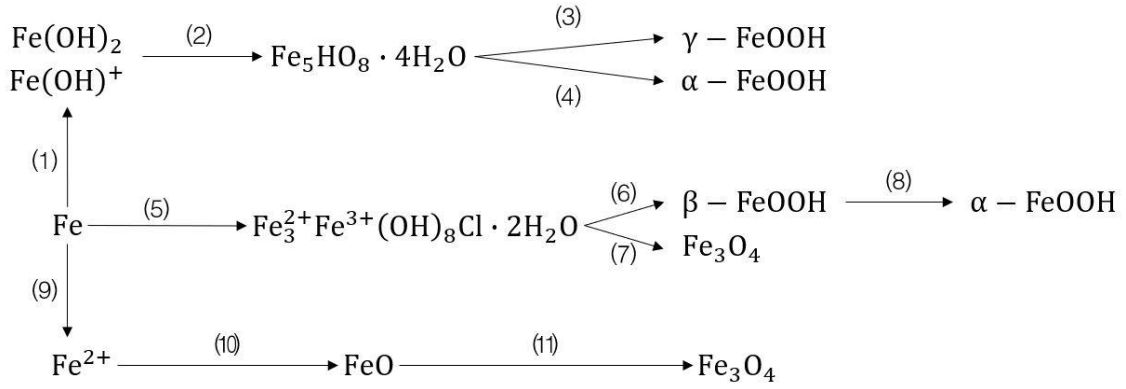

Figure 26. Process of rust formation of steel in a chloride-containing environment

The reactions of (1) and (9) indicate that the dissolved iron mainly exists in the form of Fe^{2+}, $Fe(OH)_2$ and $Fe(OH)^+$. When the solution is alkaline, $Fe(OH)_2$ and $Fe(OH)^+$ are the main components. The reaction of (2) is the formation of ferrihydrite ($Fe_5HO_8 \cdot 4H_2O$). $Fe(OH)^+$ can be absorbed on the surface of ferrihydrite, causing it to dissolve and convert to $\gamma - FeOOH$ or $\alpha - FeOOH$ (reactions (3) and (4)). (5) is the reaction of forming green rusts (GRs), which are the transition state compounds containing both ferrous and ferric iron. $\beta - FeOOH$ and Fe_3O_4 are converted from GRs, that is, the reactions (6) and (7). $\beta - FeOOH$ is unstable and quickly converted to $\alpha - FeOOH$. Reactions (10) and (11) indicate that when the corrosion rate is fast, the system is prone to lack of oxygen, and then Fe_3O_4 is formed [27].

The range of the Young's modulus of iron oxide crystals (Fe2O3 or Fe3O4) is 215–350 GPa [28]. However, rust is regarded as a granular material because the structure of rust consists of a powder grain aggregate and is more or less laminated. The interaction between the grains can significantly reduce the mechanical properties of such granular systems [29]. Therefore, this range of Young's modulus of rust is not suitable for corrosion. The Young's modulus of rust

measured by Zhao et al. [30] ranges from 47 GPa to 86 GPa. Other researchers also measured the Young's modulus of rust and got even smaller values.

According to Chapter 3.3, the topography of the 304 stainless steel sample changed a little after corrosion. The surface of the sample became darker because of the formation of rust. As the corrosion progresses, the Young's modulus gradually decreases, which coincides with the formation of the rust layer because the Young's modulus of rust is much smaller than that of uncorroded steel.

The velocity of the Rayleigh surface wave and the Young's modulus did not reduce quickly confirms the good corrosion resistance of 304 stainless steel.

4.2 Low-carbon steel sample

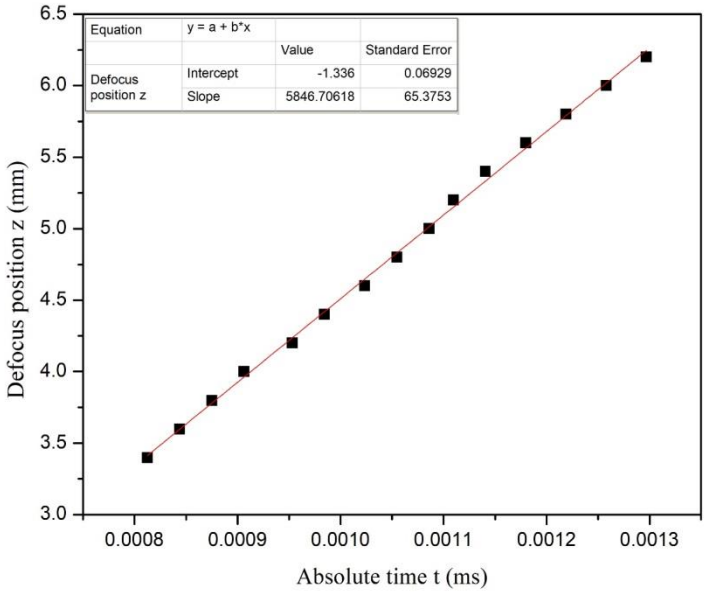

Figure 27. Defocus position vs. absolute time for the uncorroded low-carbon steel

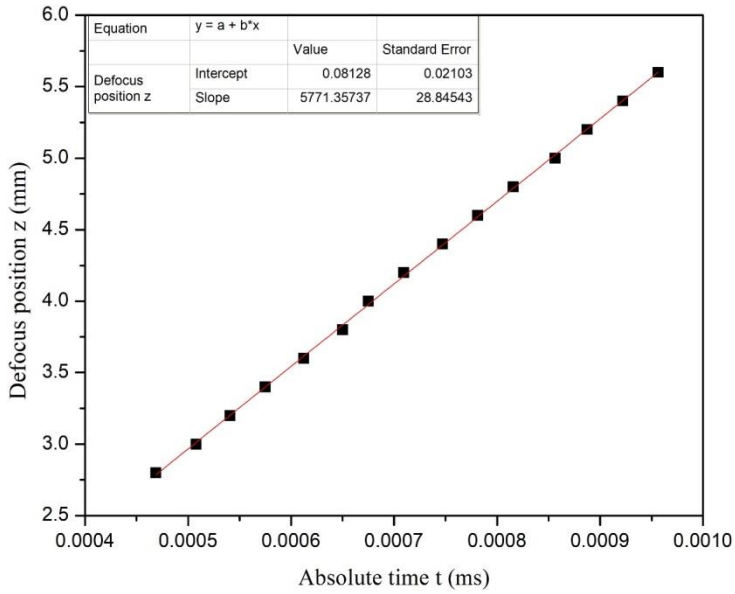

Figure 28. Defocus position vs. absolute time for the corroded low-carbon steel (5-d)

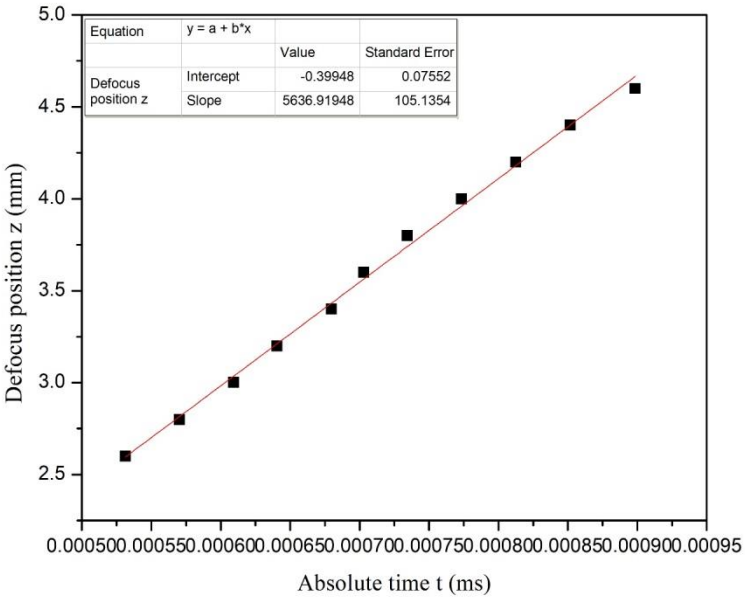

Figure 29. Defocus position vs. absolute time for the corroded low-carbon steel (10-d)

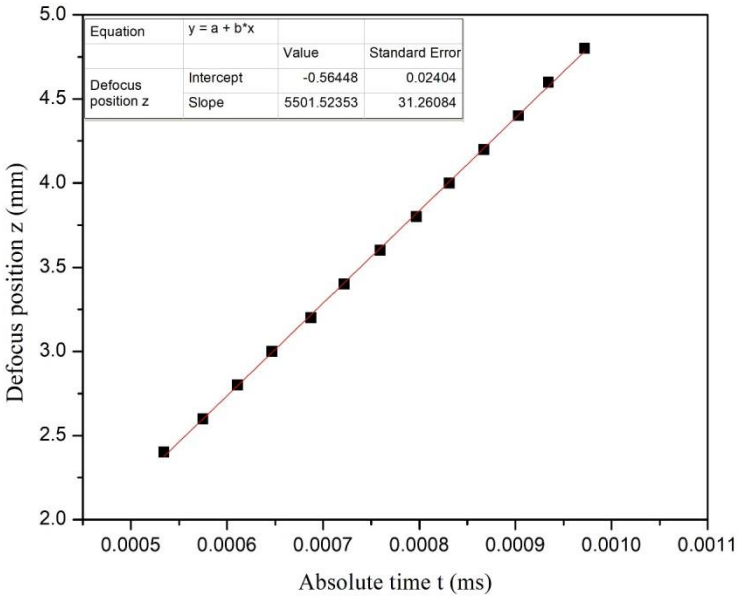

Figure 30. Defocus position vs. absolute time for the corroded low-carbon steel (15-d)

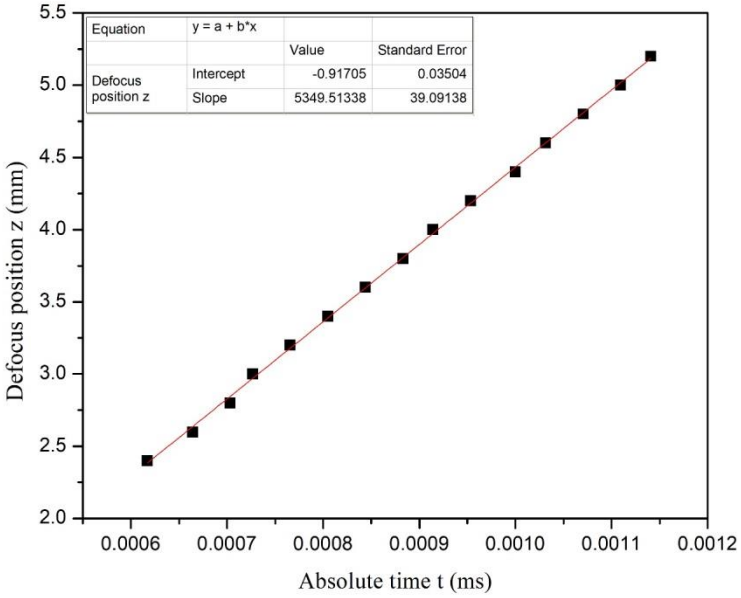

Figure 31. Defocus position vs. absolute time for the corroded low-carbon steel (20-d)

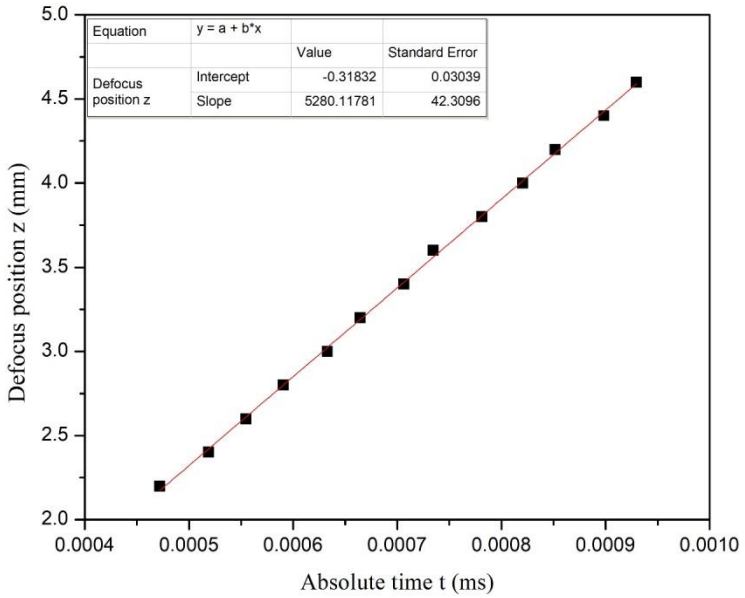

Figure 32. Defocus position vs. absolute time for the corroded low-carbon steel (25-d)

Table 5. Summary of $\frac{dz}{dt}$, v_R, v_l, v_t and E of low-carbon steel sample

Corrosion time (d)	$\frac{dz}{dt}$ (m/s)	v_R (m/s)	v_l (m/s)	v_t (m/s)	E (GPa) calculated	E (GPa) standard
0	5846.71	3041.55	5982.64	3275.05	233.32	200
5	5771.36	3023.23	5967.71	3253.11	227.04	-
10	5636.92	2990.25	5954.56	3214.57	221.97	-
15	5501.52	2956.69	5932.86	3175.99	211.59	-
20	5349.51	2943.66	5830.72	3166.29	205.69	-
25	5280.12	2900.97	5764.50	3119.30	194.38	-

The corrosion mechanism of low-carbon steel is the same with that of 304 stainless steel described in Chapter 4.1. The velocity of the Rayleigh surface wave and the Young's modulus also decrease as the corrosion time increases. The difference is that the velocity of the Rayleigh surface wave and the Young's modulus of the low-carbon steel sample both decrease faster than that of the 304 stainless steel sample. This confirms that the corrosion resistance of low-carbon steel is weaker than that of 304 stainless steel.

Compared with 304 stainless steel, the surface morphology of low-carbon steel after corrosion changed a lot as shown in Figure 16 and 17. Before cleansing, the sample was coated by a reddish-brown rust layer with a main component of Fe_2O_3; after cleansing, the surface of the sample was black with a main component of Fe_3O_4 because the surface under the rust layer was in less contact with oxygen. This indicates that the iron oxide in corroded low-carbon steel sample has more proportions than that in the corroded 304 stainless steel sample, which explains why the Young's modulus of the low-carbon steel sample decrease faster. Also, the faster the corrosion rate, the faster the Rayleigh surface wave velocity is reduced.

4.3 6061 aluminum sample

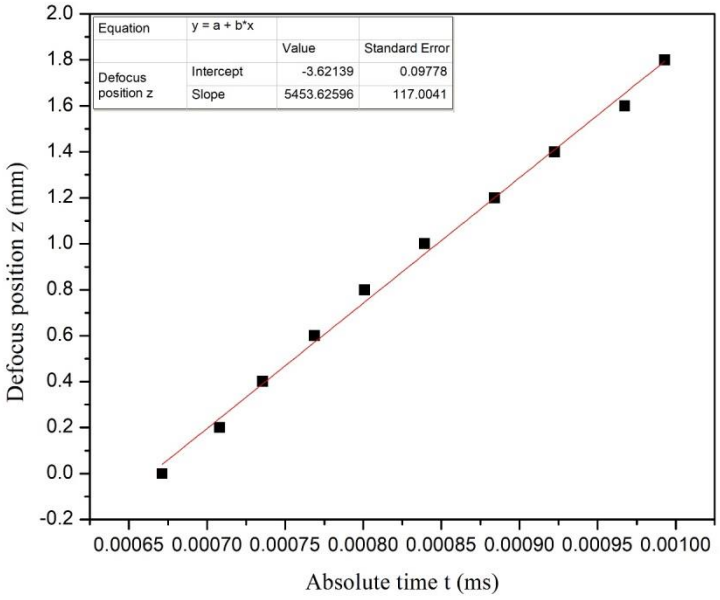

Figure 33. Defocus position vs. absolute time for the uncorroded 6061 aluminum

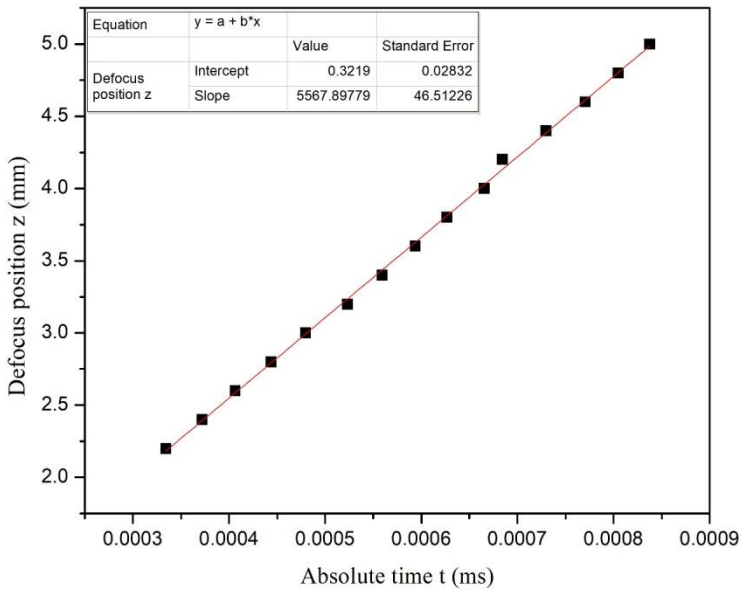

Figure 34. Defocus position vs. absolute time for the corroded 6061 aluminum (5-d)

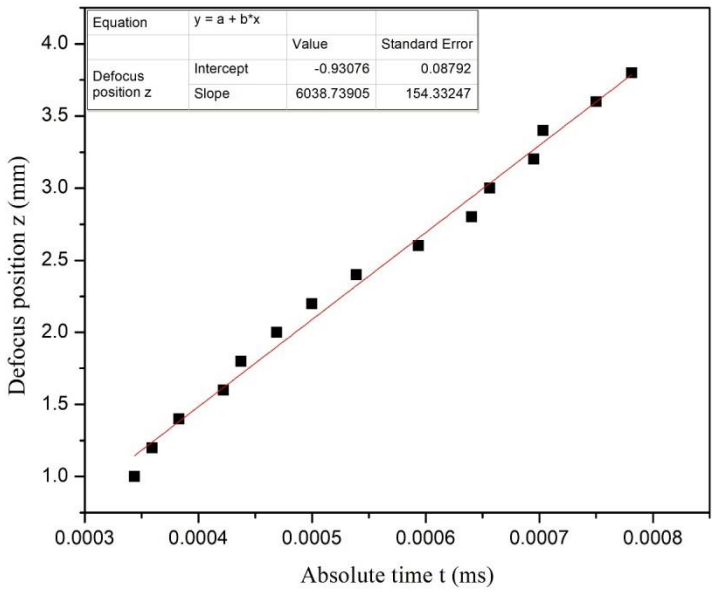

Figure 35. Defocus position vs. absolute time for the corroded 6061 aluminum (10-d)

Table 6. Summary of $\frac{dz}{dt}$, v_R, v_l, v_t and E of 6061 aluminum sample

Corrosion time (d)	$\frac{dz}{dt}$ (m/s)	v_R (m/s)	v_l (m/s)	v_t (m/s)	E (GPa) calculated	E (GPa) standard
0	5453.63	2944.72	8797.45	3103.48	73.85	68.9
5	5567.90	2973.19	8943.66	3133.02	75.55	-
10	6038.74	3087.78	9071.43	3255.48	82.22	-

The surface of the aluminum alloy is covered with a dense oxide film with a main component of Al_2O_3 at the initial stage of corrosion. As the corrosion time increases, the corrosion product layer continues to thicken. Then the corrosion products are massively stacked on the sample surface and the lower layer has corrosion pits. The sensor measurement results become

inaccurate because the surface roughness increases. Thus, we can only keep the data of 5 and 10 days of corrosion.

The velocity of the Rayleigh surface wave and the Young's modulus of 6061 Al sample increase as the corrosion time increases. This is reasonable because the Young's modulus of Al_2O_3 which is 370 GPa is much larger than that of Al which is 69 GPa [31].

In the early stage of corrosion, the corrosion resistance of aluminum is better than that of steel because the dense aluminum oxide film provides protection to the alloy. However, as time goes on, chloride ions (Cl^-) will destroy this oxide film and accelerate the corrosion of aluminum alloy. This is consistent with the actual corrosion process.

4.4 Multipurpose 110 copper sample

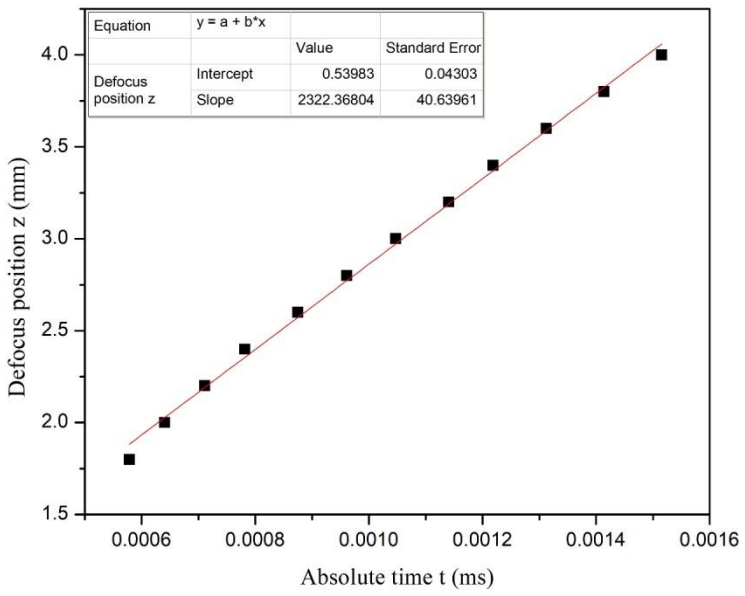

Figure 36. Defocus position vs. absolute time for the uncorroded 110 copper

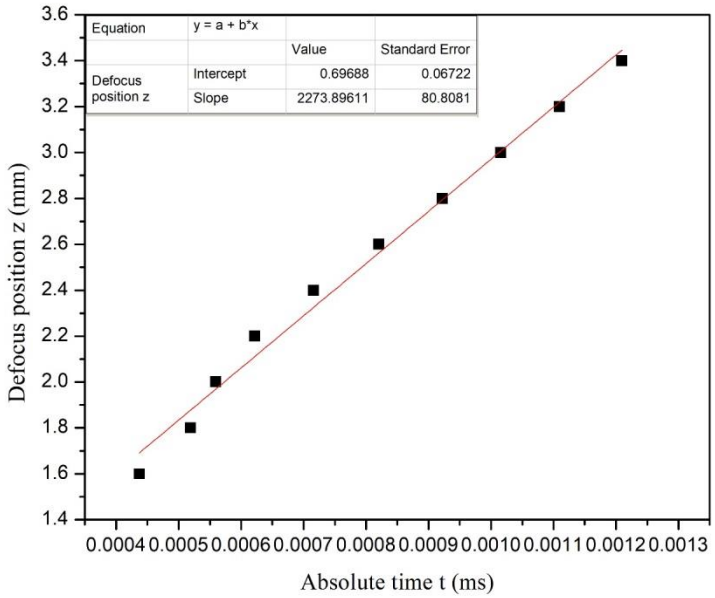

Figure 37. Defocus position vs. absolute time for the corroded 110 copper (5-d)

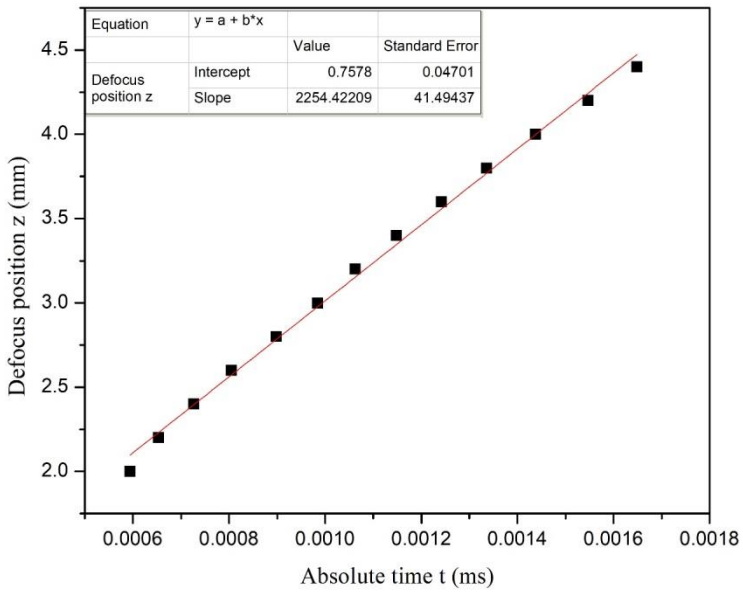

Figure 38. Defocus position vs. absolute time for the corroded 110 copper (10-d)

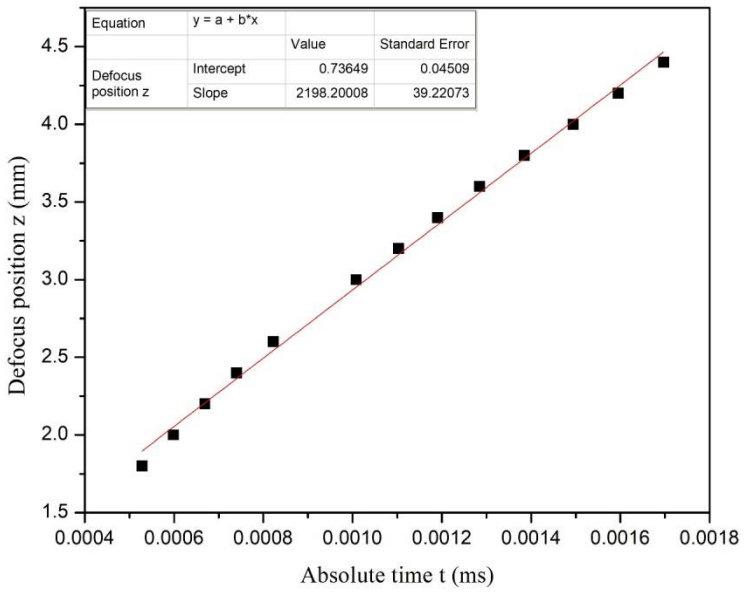

Figure 39. Defocus position vs. absolute time for the corroded 110 copper (15-d)

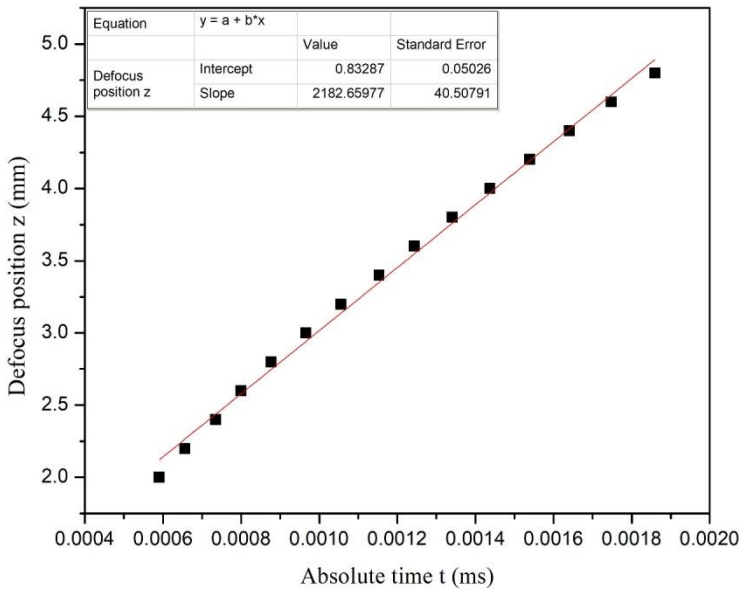

Figure 40. Defocus position vs. absolute time for the corroded 110 copper (20-d)

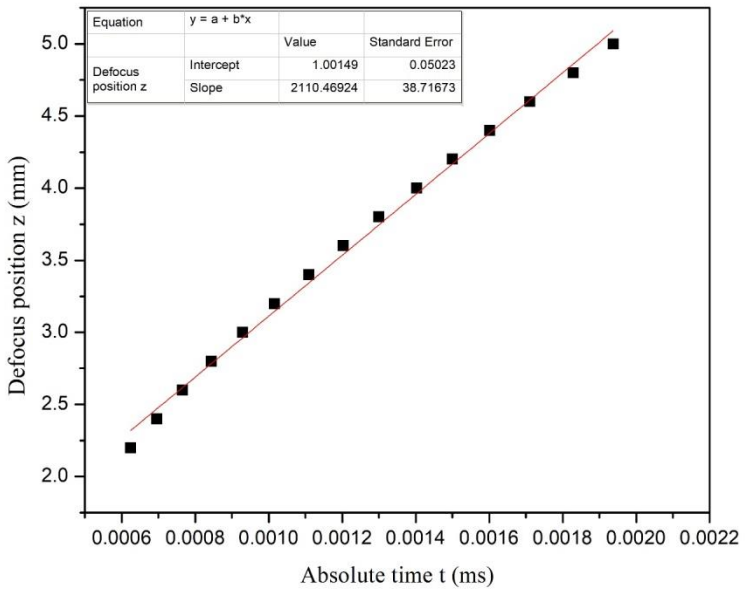

Figure 41. Defocus position vs. absolute time for the corroded 110 copper (25-d)

Table 7. Summary of $\frac{dz}{dt}$, v_R, v_l, v_t and E of multipurpose 110 copper sample

Corrosion time (d)	$\frac{dz}{dt}$ (m/s)	v_R (m/s)	v_l (m/s)	v_t (m/s)	E (GPa) calculated	E (GPa) standard
0	2322.37	2023.62	5985.71	2133.19	117.97	117
5	2273.90	2006.46	5943.55	2115.03	114.82	-
10	2254.42	1999.53	5920.35	2107.75	113.35	-
15	2198.20	1979.42	5898.60	2086.25	110.36	-
20	2182.66	1973.84	5797.33	2081.05	108.03	-
25	2110.47	1947.75	5793.46	2052.96	104.66	-

The velocity of the Rayleigh surface wave and the Young's modulus of the 110 copper sample decrease as the corrosion time increases. The Young's modulus of corrosion products, CuO and Cu_2O, are approximately 87.9 GPa [32] and 83.8 GPa [33] respectively. The Young's modulus of CuO and Cu_2O are both smaller than that of Cu which is 117 GPa. This is consistent with the reduction of the Rayleigh surface wave velocity and the Young's modulus during corrosion.

By comparing the elastic modulus changes of the four alloys, we can find that the corrosion resistance of 110 copper is stronger than that of low-carbon steel but weaker than that of 304 stainless steel. 6061 aluminum has the strongest corrosion resistance.

5.0 CONCLUSION AND FUTURE WORK

5.1 Conclusion

In this article, a PVDF line-focus ultrasonic transducer is used to measure the Rayleigh surface wave velocity and characterize the material mechanical property of four alloys: 304 stainless steel, low-carbon steel, 6061 aluminum and multipurpose 110 copper. The change of the elastic constant of the material during corrosion conforms to the corrosion mechanism and results. The velocity of the Rayleigh surface wave and the Young's modulus decrease for 304 stainless steel, low-carbon steel and multipurpose 110 copper samples, increase for 6061 aluminum sample as the corrosion time increases during the experimental period. Thus, this article may provide a feasible way to monitor corrosion conditions of alloys.

5.2 Future work

5.2.1 Transducer optimization

In real environment, the surface roughness of the alloys after corrosion is much larger than that of the samples in experiments. Thus, the frequency of the transducer should be reduced for longer wavelength in the future. Besides, the testing system takes up a lot of space which is hard to use for practical application. The portability of the system should also be considered in the future.

5.2.2 Different materials

In this article, four alloys which are all isotropic materials were tested. More materials like other alloys, ceramic materials and polymer Materials can be tested in the future. Anisotropic materials with different modulus in different direction can also be tested by this Rayleigh wave characterization method.

Bibliography

[1] Jones, K., and Hoeppner, D. W. (2006). Prior corrosion and fatigue of 2024-T3 aluminum alloy. *Corrosion Science, 48*, 3109-3122.

[2] Khaled, K. F., and Amin, M. A. (2009). Corrosion monitoring of mild steel in sulphuric acid solutions in presence of some thiazole derivatives – Molecular dynamics, chemical and electrochemical studies. *Corrosion Science, 51*, 1964-1975.

[3] Mazille, H., Rothea, R., and Tronel, C. (1995). An acoustic emission technique for monitoring pitting corrosion of austenitic stainless steels. *Corrosion Science, 37(9)*, 1365-1375.

[4] https://en.wikipedia.org/wiki/Corrosion_monitoring

[5] MIRCHEV, Y. (2016). Ultrasonic testing for general corrosion of metals and alloys. *19th World Conference on Non-Destructive Testing 2016*.

[6] Kushibiki, J., and Ishiji, H. (1985). Material Characterization by Line-Focus-Beam Acoustic Microscope. *IEEE Transactions on Sonics and Ultrasonics, Volume SU-32*.

[7] Sathish, S., Martin, R. W., and Matikas, T. E. (1999). Rayleigh wave velocity mapping using scanning acoustic microscope. *Review of Progress in Quantitative Nondestructive Evaluation, Vol. 18*.

[8] Xiang, D., Hsu, N. N., and Blessing, G. V. (1996). The design, construction and application of a large aperture lens-less line-focus PVDF transducer. *Ultrasonics, 34*, 641-647.

[9] Krautkrämer, J., and Krautkrämer, H. (1990). *Ultrasonic testing of materials*. New York: Springer-Verlag.

[10] https://en.wikipedia.org/wiki/Rayleigh_wave

[11] Tromans, D. (2011). Elastic anisotropy of HCP metal crystals and polycrystals. *IJRRAS, 6(4)*, 462.

[12] Malgrange, C. et al. (2014). *Symmetry and Physical Properties of Crystals*, Springer Science+Business Media Dordrecht.

[13] Leisure, R. G. (2017). *Ultrasonic spectroscopy: applications in condensed matter physics and materials science*. Cambridge, United Kingdom; New York, NY: Cambridge University Press.

[14] Hehl, F. W., and Itin, Y. (2002). The Cauchy Relations in Linear Elasticity Theory. *File elasticity/cauchy12.tex*

[15] Powell, R. C. (2010). *Symmetry, Group Theory, and the Physical Properties of Crystals*. New York, Dordrecht, Heidelberg, London: Springer.

[16] Viktorov, I. A. (1967). *Rayleigh and Lamb waves: physical theory and applications*. New York: Plenum Press.

[17] Royer, D., and Dieulesaint, E. (2000). *Elastic waves in solids*. Berlin, New York: Springer.

[18] https://en.wikipedia.org/wiki/Snell%27s_law

[19] https://www.nde-ed.org/EducationResources/CommunityCollege/Ultrasonics/Physics/modeconversion.htm

[20] Evans, U. R. (1960). *The corrosion and oxidation of metals; scientific principles and practical applications*. London, E. Arnold.

[21] Yamanaka, K. (1983). Surface acoustic wave measurements using an impulsive converging beam. Journal of Applied Physics, 54(8), 4323-4329.

[22] Sathish, S., Martin, R. W., and Matikas, T. E. (1999). Rayleigh wave velocity mapping using acoustic microscope. *Review of Progress in Quantitative Nondestructive Evaluation*, *18*, 2025-2030.

[23] Kim, S. -J., Noh, Y. -H., Son, M. -C., Lee, D. -J., and Kim, Y. H. (2015, Oct 12-14). Propagation Property of Leaky Surface Acoustic Wave on Monocrystalline Silicon Crystal using Large Aperture Line-Focused PVDF Transducer. *VIIIth International Workshop NDT in Progress (NDTP2015)*.

[24] Yang, C. -H. (1998). Characterization of piezoelectrics using line-focus transducer. *Review of Progress in Quantitative Nondestructive Evaluation*, *17*, 177-184.

[25] Ji, C. (2017). Corrosion evaluation of additive manufacture metal alloy by nondestructive line-focused transducer. University of Pittsburgh.

[26] Nazarchuk, Z. et al. (2017). *Acoustic Emission*, Foundations of Engineering Mechanics. Springer International Publishing.

[27] Ouglova, A., Berthaud, Y., Francois, M., and Foct, F. (2006). *Corrosion Science*, *48*, 3988-4000.

[28] Samsonov, G. V. (1973). *The oxide handbook*. New York: IFI/Plenum.

[29] Liu, Q., and Su, R. K. L. (2018). A displacement-based inverse analysis method to estimate in-situ Young's modulus of steel rust in reinforced concrete. *Engineering Fracture Mechanics*, *192*, 114-128.

[30] Zhao, Y., Dai, H., and Jin, W. (2012). A study of the elastic moduli of corrosion products using nano-indentation techniques. *Corrosion Science*, *65*, 163-168.

[31] Saif, M. T. A., Zhang, S., Haque, A., and Hsia, K. J. (2002). Effect of native Al_2O_3 on the elastic response of nanoscale Al films. *Acta Materialia*, *50*, 2779-2786.

[32] Yao, B., Zhou, X., Liu, M., Yu, J., Cao, J., and Wang, L. (2018). First-principles calculations on phase transformation and elastic properties of CuO under pressure. *Journal of Computation Electronics*, *17*, 1450-1456.

[33] Ruiz, E., and Alvarez, S. (1997). Electronic structure and properties of Cu_2O. *PHYSICAL REVIEW B*, *56(12)*, 7189-7196.